Journal of
Mechanics of
Materials and Structures

**STRESS AND BUCKLING ANALYSES OF LAMINATES
WITH A CUTOUT USING A {3, 0}-PLATE THEORY**

Atila Barut, Erdogan Madenci and Michael P. Nemeth

Volume 6, No. 6   July–August 2011

msp

STRESS AND BUCKLING ANALYSES OF LAMINATES
WITH A CUTOUT USING A {3, 0}-PLATE THEORY

Atila Barut, Erdogan Madenci and Michael P. Nemeth

A semianalytical solution method to predict stress field and structural bifurcation in laminates having a cutout by employing a simple {3, 0}-plate theory is presented. The stress analysis includes both in-plane and bending stress fields. In this theory, the in-plane and out-of-plane displacement fields are respectively assumed in the forms of cubic and uniform through-the-thickness expansions. The cubic expansion ensures the correct behavior of transverse shear deformations while satisfying the condition of zero transverse shear stresses at the laminate faces. The equations of equilibrium for the stress and buckling analysis are derived based on the principle of stationary potential energy. Comparison against the classical laminate and {1, 2}-plate theories proves this semianalytical method credible.

1. Introduction

Understanding the behavior of laminated composite plates is an important part of designing ultralightweight, high-performance aircraft structures. Typically, these structures are relatively thin and are designed by using analyses based on the classical laminated plate theory (CLPT) [Jones 1975]. However, there are instances in which using a higher-order refined theory becomes unavoidable in order to include accurately the effects of transverse shear flexibility on the structural response to obtain an initial design that is conservative or to verify margins of safety of a current design. The refined theories can be classified as *equivalent single-layer*, *layer-wise*, *zigzag*, and *variational asymptotic*. Although there are many different refined plate theories, they have not found wide acceptance in standard industry design practices because of the extensive experience base with CLPT. Thus, the focus of this study is to formulate new, advanced special-purpose analysis and design tools by using a refined plate theory that contains CLPT as an explicit, well-defined subset of the governing equations. A refined theory of this type may be useful in developing nondimensional design parameters that characterize the effects of transverse shear deformation and in extending the current design practice accepted by industry in a cautious building-block manner. Moreover, company-validated legacy computer codes can be retained and updated to include the effects of transverse shear flexibility with only some additional validation costs.

Each of the many refined theories for laminated composite plates has its own merits and range of validity associated with a given class of problems. Obviously, the choice of which theory to use depends on the nature of response characteristics. For example, for global response phenomena, such as elastic buckling and vibration response, that are not characterized by short wavelengths, it is likely that an equivalent single-layer theory would be sufficiently adequate. Attributes of several of these theories have been investigated and discussed in works such as [Liu and Li 1996; Reddy 1997; Altenbach 1998;

Keywords: composite, cutout, transverse shear deformation, bending, buckling.

Barut et al. 2002; Yu and Hodges 2004; Demasi and Yu 2009]. A recent extensive discussion of the layer-wise and zigzag theories can be found in [Tessler et al. 2009].

In the development of special-purpose analysis tools that account for the effects of transverse shear flexibility for use in preliminary designs, rapid navigation of the design-parameter space is desired. As a result, computational efficiency is a major concern. This desire is driven by the wide range of laminated composite constructions available and the potential weight savings that can be obtained through laminate tailoring. Thus, it follows logically that a relatively simple equivalent single-layer refined plate theory is generally the starting point in the enhancement of legacy analysis tools that are based on CLPT. However, many of these theories, such as the first-order shear deformation theory (FSDT) first derived by Reissner [1944; 1945], do not contain the dependent kinematic variables of CLPT as an explicit subset. In the parlance of functional analysis, when the dependent kinematic variables of CLPT appear explicitly as a subset, the dependent kinematic variables of the refined theory possess a well-conditioned, linearly independent basis that also spans the CLPT subspace — analytically and computationally. According to [Shimpi 1999; Ray 2003], this attribute eliminates the numerical ill-conditioning that causes shear locking in finite element analyses of thin shear-deformable plates that are based on theories that use the rotations of the material line element, which is normal to the plate midplane, as dependent variables. The ill-conditioning arises from the fact that CLPT solutions are not recovered directly, but in an asymptotic sense, as the plate thickness is reduced and the transverse shear stiffness is increased.

There are laminated-plate theories that account for the effects of transverse shear flexibility and that do contain the dependent kinematic variables of CLPT as an explicitly defined subset. Reddy [1990] presented a review of all the existing third-order theories and showed that they are actually special cases of his third-order plate theory [Reddy 1984], in which the in-plane displacement components are cubic through-the-thickness expansions, yielding a quadratic variation of transverse shear strains, and the transverse displacement component is constant through the thickness, excluding the transverse normal deformations. While this formulation is applicable to plates with simply supported boundary conditions [Sun and Hsu 1990], it yields physically unacceptable zero transverse shear strains when both in-plane displacement components are fixed along the plate edges, as pointed out in [Krishna Murty 1987]. The problem was remedied by decomposing the transverse displacement component into separate parts for the displacements associated with bending and shear deformations. This has been applied successfully to stress [Krishna Murty 1987; Iyengar and Chakraborty 2004], buckling [Senthilnathan et al. 1987], and large deflection analyses [Reddy 1987; 1990; Singh et al. 1994] of isotropic and laminated plates. An alternative to decomposing the transverse displacement field in order to avoid zero transverse shearing along fixed-edge boundaries was proposed in [Voyiadjis and Shi 1991] for thick cylindrical shells and later reduced to plate kinematics in [Shi 2007]. In this alternative approach, average displacement and slope variables were utilized that produce an equivalent transverse shear strain energy density. The present study adopts the use of average displacements and slopes around plate boundaries by using Reissner's weighted-average displacement and slope definitions [Reissner 1944; 1945].

Other forms of higher-order theories for plates and shells have also been proposed. For example, [Soldatos and Timarci 1993; Timarci and Aydogdu 2005] employed higher-order theories based on polynomial, trigonometric, hyperbolic, and exponential expansions of in-plane displacements through the thickness and compared their relative accuracy in stress and buckling analyses of plates and shells. Shu and Sun [1994] introduced a third-order shear deformation theory that satisfies continuity of in-plane

displacements and transverse shear stresses between adjacent layers. However, their representation of the displacement variables resembles that of FSDT. Recently, Ray [2003] extended the zeroth-order shear deformation theory (ZSDT) of Shimpi [1999] to perform vibration analysis of simply supported laminated composites. It can be shown that the ZSDT of Shimpi and Ray is a special case of the form introduced in [Timarci and Aydogdu 2005]. The present study employs the kinematics of Shimpi's ZSDT because of its accuracy and simplicity in predicting the responses of laminated plates [Ray 2003]. Because of the cubic and constant through-the-thickness expansions used for the representation of, respectively, the in-plane and transverse displacement components of ZSDT, we use the term {3, 0}-*plate theory*. Notation of this type was originally introduced in [Tessler 1993].

Pertinent to the focus of the present refined single-layer theory, several results have been presented in the literature that show the relative accuracy of third-order plate theories. For example, Reddy [1997] presented results for bending, vibration, and buckling of flat rectangular laminated plates using his third-order plate theory. He presented solutions for simply supported, square, symmetric, and antisymmetric cross-ply laminates under sinusoidal pressure distributions. Transverse deflection of laminates with thickness-to-length ratios (h/L) as large as $\frac{1}{4}$ were compared against the exact elasticity solutions, CLPT and FSDT. Ramm [2000] presented the historical evolution of the FSDT and introduced a second-order plate theory whose kinematics account for both uniform and linear expansion modes in the thickness direction in addition to the transverse shear strains. In particular, in [Noor and Malik 2000] four modeling approaches were studied, based on first-order, second-order, third-order, and discrete-layer theories. Rohwer et al. [2001] presented the existing higher-order theories that are in polynomial form as truncated power series expansions of displacements with constant coefficients. The constant coefficients and truncation of the power series were determined based on term-by-term matching of the power series with the corresponding kinematic representation. They also introduced a generic fifth-order plate theory. Although this theory does not generally satisfy shear and normal traction-free boundary conditions at plate surfaces, it yields more accurate results than the third-order theories for simply supported orthotropic, symmetric, and nonsymmetric cross-ply laminates. In [Bosia et al. 2002] the validity of CLPT and FSDT were investigated by comparing numerical predictions of laminates under bending against experimental measurements. The results indicate that both CLPT and FSDT fail to capture the correct response for plates whose span-to-thickness ratio is lower than 25.

In [Tessler and Saether 1991; Tessler 1993] a second-order shear-deformation theory was introduced that includes quadratic expansions of transverse shear deformations and a linear expansion of transverse normal deformations through the thickness. Similarly, in [Reddy 1990; Barut et al. 2002] third-order plate theories were formulated for thick laminates, taking into account both transverse normal and shear deformations, as well as cubic variation of in-plane deformations. Also, the survey of the existing higher-order plate theories [Ghugal and Shimpi 2002] focuses on first-order, second-order, and various forms of higher-order shear deformation theories that have been developed for isotropic and laminated plates.

None of the previous studies considered laminates with cutouts, which can cause local gradients in the stress and strain fields that may lead to premature structural failure, especially due to structural buckling. Thus, it is important to understand how cutouts affect the transverse shear flexibility of laminates. Therefore, the objective of the present study is to derive the governing equations of a {3, 0}-plate theory for stress and buckling analysis of laminated composite plates under general loading and boundary conditions. This plate theory contains the dependent variables of CLPT as a proper subspace, provides

the quadratic variation of transverse shear stresses through the thickness of the laminate, satisfies the condition of zero transverse shear stresses on the top and bottom surfaces of the laminate, and does not require a transverse shear correction factor.

This study presents a semianalytical solution method for predicting the bending and buckling behavior of a moderately thick laminate with a cutout. While employing the {3, 0}-plate theory, the present approach utilizes the principle of stationary potential energy to derive the governing equations for bending deformation and structural bifurcation. The solutions of these governing equations are obtained by employing global and local function sets that mathematically take into account the presence of cutouts and general boundary conditions. Two sets of results are presented for selected structural configurations with a cutout. These sets are linear-bending analysis results, which address the accurate representation of local through-the-thickness effects, and buckling analysis results, which address global stiffness-critical effects. For both sets of results, all deformations are presumed to be elastic.

2. Overview of the {3, 0}-plate theory

The nonlinear plate theory used in the present study is based on the kinematic equations presented in [Sun and Hsu 1990] and is a special case of the formulation presented in [Soldatos and Timarci 1993; Timarci and Aydogdu 2005]. In particular, the in-plane and transverse displacement fields of a material point (x, y, z) are expressed in Cartesian coordinates (see Figure 1 on page 832) as

$$U_x(x, y, z) = u_x(x, y) - zu_{z,x}(x, y) + \Lambda(z)\Phi_{xz}(x, y), \tag{1a}$$

$$U_y(x, y, z) = u_y(x, y) - zu_{z,y}(x, y) + \Lambda(z)\Phi_{yz}(x, y), \tag{1b}$$

$$U_z(x, y, z) = u_z(x, y), \tag{1c}$$

where the displacements U_x, U_y, and U_z are associated with the x, y, and z-directions, respectively. The functions u_x and u_y represent the in-plane displacements, and u_z represents the out-of-plane displacement of the point $(x, y, 0)$ on the laminate midplane; a subscript after a comma denotes partial differentiation. Inspection of these equations reveals that the kinematic equations of CLPT appear explicitly. The function $\Lambda(z)$ is selected to satisfy the traction-free boundary conditions on shear stresses at the outer, bounding surfaces of a laminate and to satisfy the conditions $U_x(x, y, 0) = u_x(x, y)$ and $U_y(x, y, 0) = u_y(x, y)$. As noted in [Timarci and Aydogdu 2005], the choice of $\Lambda(z)$ is not unique. In the present study, $\Lambda(z)$ is specified as a cubic through-the-thickness distribution, which is one of the special cases examined by Timarci and Aydogdu. Because the corresponding functional representations of the displacement fields consist of cubic polynomial expansions in the through-the-thickness coordinate z for the in-plane displacements and no expansion for the out-of-plane displacement, the theory is denoted herein as a {3, 0}-plate theory based on the notation of [Tessler 1993].

The kinematic assumptions given by (1) are modified forms of those given in [Ray 2003]. In particular, the unknown functions $\Phi_{xz}(x, y)$ and $\Phi_{yz}(x, y)$ are, generally, not the stiffness-weighted transverse shear stress resultants of CLPT, used by Ray and initially suggested in [Shimpi 1999]. This representation permits the application of the plate theory to the entire class of laminated plates and is consistent with full coupling of the transverse shearing stress and transverse shearing strains, through the constitutive equations.

Reddy [1990] showed that the {3, 0} theory presented herein can be obtained from his {3, 0} theory by a simple transformation of the dependent kinematic variables. As a result, the inherent physical accuracy of the two {3, 0} theories are expected to be identical. However, the computational attributes are likely to be quite different, particularly for large relative values of the transverse shear stiffnesses.

The boundary conditions associated with the {3, 0}-plate theory include terms arising from the presence of higher-order in-plane deformation modes. It is difficult to interpret and associate the higher-order terms, Φ_{xz} and Φ_{yz}, with commonly used boundary displacements and slopes. In this study, this difficulty is avoided by introducing independent boundary displacements, $\tilde{U}_\alpha$, with $\alpha = x, y, z$. Based on the kinematics of the Mindlin plate theory, these boundary displacements are defined as

$$\tilde{U}_x(x, y, z) = \tilde{u}_x(x, y) - z\tilde{\vartheta}_x(x, y), \tag{2a}$$

$$\tilde{U}_y(x, y, z) = \tilde{u}_y(x, y) - z\tilde{\vartheta}_y(x, y), \tag{2b}$$

$$\tilde{U}_z(x, y, z) = \tilde{u}_z(x, y), \tag{2c}$$

in which $\tilde{u}_x(x, y)$, $\tilde{u}_y(x, y)$, and $\tilde{u}_z(x, y)$ represent the weighted-average displacements and $\tilde{\vartheta}_x(x, y)$ and $\tilde{\vartheta}_y(x, y)$ rotations. Their representation in terms of the kinematics of the {3, 0} theory presented herein is achieved by minimizing the error between U_α and $\tilde{U}_\alpha$ ($\alpha = x, y, z$), that is,

$$\min\left[\int_{-h/2}^{h/2} \{(\tilde{U}_x - U_x)^2 + (\tilde{U}_y - U_y)^2 + (\tilde{U}_z - U_z)^2\}\, dz\right]. \tag{3}$$

The minimization of (3) with respect to the independent quantities, $\tilde{u}_\alpha(x, y)$ with $\alpha = x, y, z$ and $\tilde{\vartheta}_\beta(x, y)$ with $\beta = x, y$, leads to the following weighted averages:

$$(\tilde{u}_x, \tilde{u}_y, \tilde{u}_z) = \frac{1}{h}\int_{-h/2}^{h/2} (U_x, U_y, U_z)\, dz, \qquad (\tilde{\vartheta}_x, \tilde{\vartheta}_y) = \frac{12}{h^3}\int_{-h/2}^{h/2} z(U_x, U_y)\, dz. \tag{4}$$

Substituting U_x, U_y, and U_z from (1) into these equations results in the following explicit forms given in terms of the kinematics of the {3, 0} theory:

$$\tilde{u}_\alpha(x, y) = u_\alpha(x, y) \qquad \text{with} \quad \alpha = x, y, z, \tag{5a}$$

$$\tilde{\vartheta}_\beta(x, y) = u_{z,\beta}(x, y) - \frac{6}{5h}\Phi_{\beta z}(x, y) \qquad \text{with} \quad \beta = x, y. \tag{5b}$$

Hence, this representation of the boundary displacements and slopes is the least-squares equivalent of the {3, 0} theory kinematics along the boundary.

The nonlinear strain-displacement relations used in the present study are based on the Green–Lagrange strains of elasticity theory, simplified for a flexible plate-like solid exhibiting small strains and moderately small rotations by using the von Kármán assumptions [Fung and Tong 2001].

The corresponding nonlinear plate strains are obtained by substituting (1) into the simplified Green–Lagrange strains. Work-conjugate stress resultants are identified by substituting the plate strains into the strain energy and then reducing it to a two-dimensional quantity by through-the-thickness integration. The laminate constitutive equations are obtained by substituting the expressions for the laminate strains into the stress-strain relations for a generally orthotropic material, in a state of plane stress, and by then

substituting the resulting equations for the stresses into the definitions of the stress resultants and performing the through-the-thickness integrations. The nonlinear equilibrium equations and the corresponding boundary conditions are obtained by taking the variation of the total potential energy of the laminate and using Green's integral theorem to enforce the fundamental theorem of the calculus of variations.

3. Problem description

The general boundary-value problem considered in the present study consists of a rectangular laminate with an elliptical cutout that is located arbitrarily (Figure 1). The cutout has a semimajor axis and a semiminor axis with lengths $2a$ and $2b$, respectively. As shown in Figure 1, the local Cartesian coordinate system (x', y', z'), whose origin is located at the center of the cutout, coincides with the principal coordinates of the elliptical cutout. The global structural coordinates are denoted by (x, y, z), and the orientation of the cutout with respect to the global horizontal axis is defined by the angle ψ. The laminate is made of K specially orthotropic layers, and each layer has an orientation angle, θ_k, that is defined with respect to the x-axis (see Figure 1). The total laminate thickness is denoted by h. Each layer has a thickness of h_k; elastic moduli E_{11}, E_{22}, and E_{33}; shear moduli G_{12}, G_{23}, and G_{31}; and Poisson's ratios ν_{12}, ν_{23}, and ν_{31}; the subscripts 1, 2, and 3 represent the fiber, transverse, and thickness directions, respectively.

A special, practical set of loading conditions are considered in the present study. As shown in Figure 1, Γ_σ represents the laminate edges that are traction free, and Γ_u denotes the part of the laminate boundary
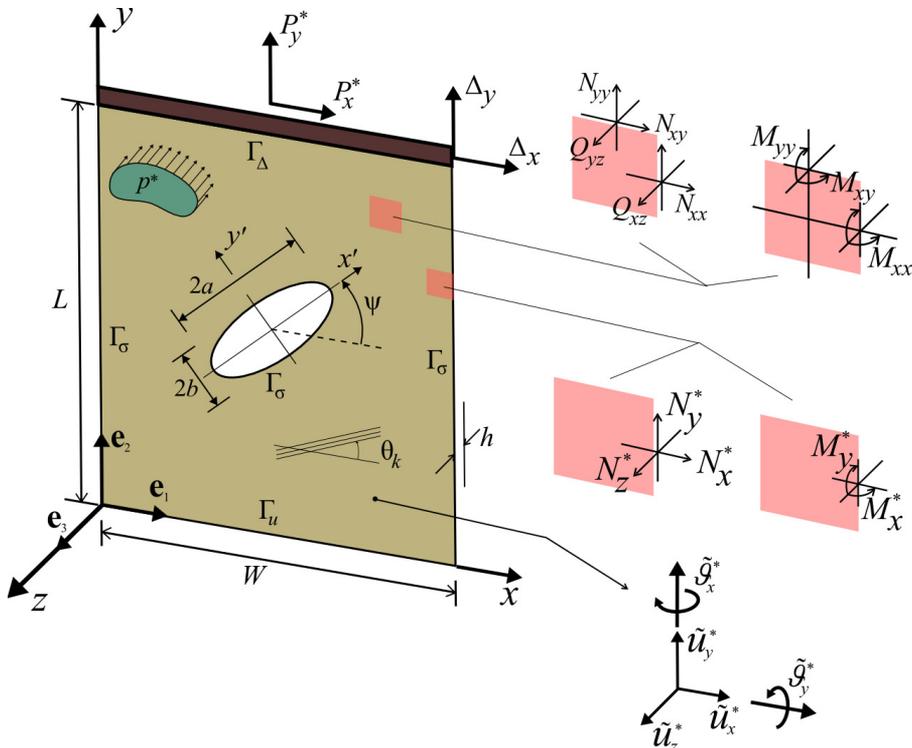
Figure 1. Description of geometry and loading of composite plate with an elliptical cutout.

that is kinematically restrained. The laminate boundary on which the kinematics of the boundary is constrained by uniform edge displacements is represented by Γ_Δ. This boundary can be clamped or simply supported against bending while allowing for uniform in-plane edge displacements. As depicted in Figure 1, uniform edge displacement is achieved in the present study through use of a rigid load fixture (rigid bar) that is subjected to concentrated edge forces. This approach is used to represent the most commonly employed experimental loading conditions. Throughout this paper, a variable with the superscript "∗" is treated as a *known quantity*, arising from the externally applied loads or from prescribed displacements and rotations.

The laminate can be subjected to an arbitrary lateral distributed load of $p^*(x, y)$ pointing in the negative z-direction, as shown in Figure 1. The positive-valued stress and moment resultants of applied boundary tractions, (N_x^*, N_y^*, N_z^*) and (M_x^*, M_y^*), are applied along the edges as shown in Figure 1. The concentrated forces, P_x^* and P_y^*, applied to the ends of the laminate through a rigid end-bar, as shown in Figure 2, lead to uniform edge displacements with *unknown* magnitudes Δ_x and Δ_y.

The prescribed edge displacements on the midplane $(\tilde{u}_x^*, \tilde{u}_y^*, \tilde{u}_z^*)$ and edge slopes $(\tilde{\vartheta}_x^*, \tilde{\vartheta}_y^*)$ on the x-z and y-z planes, respectively, are imposed as

$$\tilde{u}_i(x, y) = \tilde{u}_i^* \quad (i = x, y, z),$$
$$\tilde{\vartheta}_i = \tilde{\vartheta}_i^* \quad (i = x, y), \tag{6}$$

where $\tilde{u}_x$, $\tilde{u}_y$, and $\tilde{u}_z$ denote the weighted-average boundary displacements and $\tilde{\vartheta}_x$ and $\tilde{\vartheta}_y$ are the weighted-average slope quantities.

As shown in Figure 2, the kinematic boundary conditions are imposed by employing elastic spring supports. Zero-valued displacement and rotation kinematic boundary conditions are enforced in an indirect manner by specifying values for the spring stiffnesses that are large compared to the corresponding laminate stiffnesses. This approach effectively yields a prescribed kinematic boundary condition in the limit as the relative stiffness of the spring becomes much greater than that of the corresponding laminate stiffness. Similarly, values for the spring stiffnesses can be selected corresponding to a given uniform
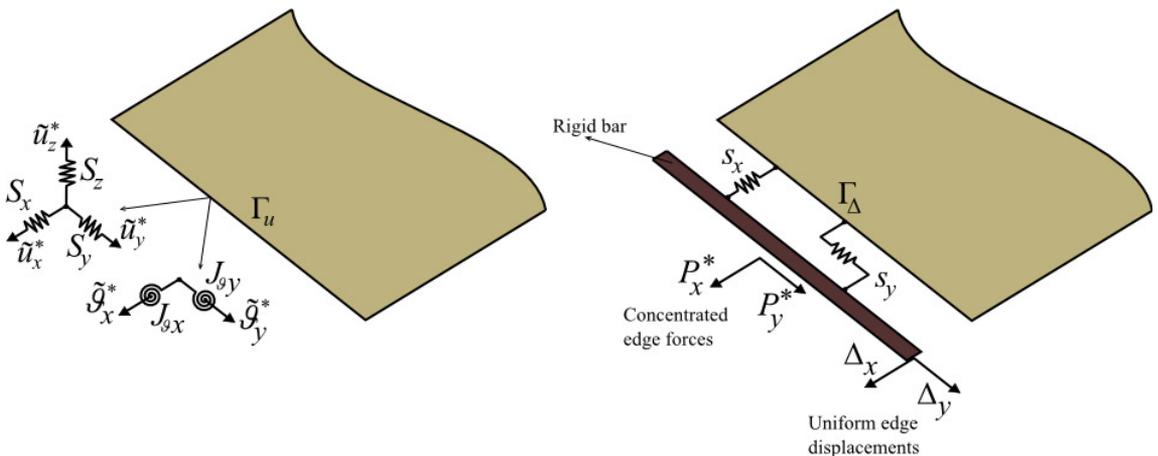
Figure 2. Distributed elastic spring supports along the edges of a laminate.

elastic restraint along an edge, similar to that provided by a rigid end-bar. This capability is important and useful because in some test fixtures, or actual structures, the edge supports may not be stiff enough to simulate a fully clamped boundary condition or flexible enough to simulate a simply supported boundary condition. The extensional and rotational springs have constants S_x, S_y, and S_z associated with the edge displacements and $J_{\vartheta x}$ and $J_{\vartheta y}$ with the slopes. In addition, a rigid end-bar is linked to the plate edge through extensional springs in the directions normal and tangent to the boundary with stiffness values of s_x and s_y. The specification of a sufficiently large value of spring stiffness for s_x and s_y causes the plate edge to behave as a rigid end-bar with uniform displacements, Δ_x and Δ_y. Conversely, a sufficiently small spring stiffness between the plate edge and the rigid end-bar eliminates the presence of a rigid end-bar. In the case of buckling analysis, this type of edge support, commonly used in buckling experiments, permits the determination of the end shortening of the plate.

4. Nonlinear equations of the {3, 0}-plate theory

The nonlinear equations of the plate theory are derived by considering the variation of the total potential energy of the laminate. In the present study, the total potential energy consists of the potential energy of the elastic spring supports in addition to the internal strain energy of deformation and the work of the applied loads.

Strain field and potential energy. The internal strain energy of deformation is generated by the presence of a strain field within a laminate. For the plate kinematics defined by (1), the corresponding nonlinear strain-displacement relations that correspond to small strains and moderate rotations are given by

$$\boldsymbol{\epsilon} = \boldsymbol{\epsilon}^0 + z\boldsymbol{\kappa}^0 + \Lambda(z)\boldsymbol{\Gamma}^0, \tag{7a}$$

$$\boldsymbol{\gamma} = \Lambda'(z)\boldsymbol{\Phi}, \tag{7b}$$

where the vectors $\boldsymbol{\epsilon}$, $\boldsymbol{\gamma}$, $\boldsymbol{\epsilon}^0$, $\boldsymbol{\kappa}^0$, $\boldsymbol{\Gamma}^0$, and $\boldsymbol{\Phi}$ are defined as

$$\boldsymbol{\epsilon}^T = \{\epsilon_{xx}, \epsilon_{yy}, \gamma_{xy}\}, \qquad \boldsymbol{\gamma}^T = \{\gamma_{xz}, \gamma_{yz}\}, \tag{7c}$$

$$\boldsymbol{\epsilon}^{0^T} = \left\{ \left[u_{x,x} + \tfrac{1}{2}(u_{z,x})^2 \right], \left[u_{y,y} + \tfrac{1}{2}(u_{z,y})^2 \right], (u_{x,y} + u_{y,x} + u_{z,x} u_{z,y}) \right\}, \tag{7d}$$

$$\boldsymbol{\kappa}^{0^T} = -\{u_{z,xx}, u_{z,yy}, 2u_{z,xy}\}, \quad \boldsymbol{\Gamma}^{0^T} = \{\Phi_{xz,x}, \Phi_{yz,y}, (\Phi_{xz,y} + \Phi_{yz,x})\}, \quad \boldsymbol{\Phi}^T = \{\Phi_{xz}, \Phi_{yz}\}. \tag{7e}$$

The prime mark in (7b) denotes differentiation with respect to the through-the-thickness coordinate z. The transverse normal strain, ϵ_{zz}, is zero-valued, consistent with assumption of a uniform through-the-thickness out-of-plane displacement specified by (1c). In addition, defining average transverse shearing strains γ_{xz}^0 and γ_{yz}^0 by

$$\boldsymbol{\gamma}^0 = \begin{Bmatrix} \gamma_{xz}^0 \\ \gamma_{yz}^0 \end{Bmatrix} = \frac{1}{h} \int_{-h/2}^{+h/2} \begin{Bmatrix} \gamma_{xz} \\ \gamma_{yz} \end{Bmatrix} dz, \tag{8}$$

where h denotes the uniform thickness of the plate, gives

$$\boldsymbol{\gamma}^0 = \frac{1}{h} \left(\Lambda\left(\frac{h}{2}\right) - \Lambda\left(-\frac{h}{2}\right) \right) \begin{Bmatrix} \Phi_{xz} \\ \Phi_{yz} \end{Bmatrix}. \tag{9}$$

Inspection of (7b) reveals that the transverse shearing strains vanish at the bounding surfaces of the plate given by $z = \pm h/2$ provided that

$$\Lambda'(h/2) = \Lambda'(-h/2) = 0. \tag{10}$$

The strain energy of a laminate is obtained by substituting the expressions for the strains in Equations (7) into the strain energy expression for a three-dimensional elastic solid and performing through-the-thickness integration of the resulting equations. This process yields the strain energy of a laminate as

$$U = \frac{1}{2} \int_A (\boldsymbol{N}^T \boldsymbol{\epsilon}^0 + \boldsymbol{M}^T \boldsymbol{\kappa}^0 + \boldsymbol{F}^T \boldsymbol{\Gamma}^0 + \boldsymbol{f}^T \boldsymbol{\Phi}) \, dx \, dy, \tag{11}$$

with

$$\boldsymbol{N}^T = \{N_{xx}, N_{yy}, N_{xy}\}, \quad \boldsymbol{M}^T = \{M_{xx}, M_{yy}, M_{xy}\}, \quad \boldsymbol{F}^T = \{F_{xx}, F_{yy}, F_{xy}\}, \quad \boldsymbol{f}^T = \{f_{xz}, f_{yz}\}, \tag{12}$$

where the definitions of the stress resultants appearing in this expression, N_{ij}, M_{ij}, and F_{ij} with $i, j = x, y$ and f_{iz} with $i = x, y$, are given in Appendix A. It is convenient to express (11) in the following compact form:

$$U = \frac{1}{2} \int_A \boldsymbol{s}^T \boldsymbol{e} \, dA, \tag{13}$$

where $\boldsymbol{s}$ and $\boldsymbol{e}$ are vectors of the stress and strain resultants given by

$$\boldsymbol{s}^T = \{\boldsymbol{N}^T, \boldsymbol{M}^T, \boldsymbol{F}^T, \boldsymbol{f}^T\}, \tag{14a}$$

$$\boldsymbol{e}^T = \{\boldsymbol{\epsilon}^{0^T}, \boldsymbol{\kappa}^{0^T}, \boldsymbol{\Gamma}^{0^T}, \boldsymbol{\Phi}^T\}. \tag{14b}$$

For the elastic materials considered herein, the stress resultant vector $\boldsymbol{s}$ is related to the strain resultant vector $\boldsymbol{e}$ through the constitutive matrix $\boldsymbol{C}$ as

$$\boldsymbol{s} = \boldsymbol{C}\boldsymbol{e}, \tag{15}$$

in which

$$\boldsymbol{C} = \begin{bmatrix} \boldsymbol{A} & \boldsymbol{B} & \boldsymbol{E} & \boldsymbol{0} \\ & \boldsymbol{D} & \boldsymbol{F} & \boldsymbol{0} \\ & & \boldsymbol{H} & \boldsymbol{0} \\ & & & \boldsymbol{G} \end{bmatrix}. \tag{16}$$

The submatrices $\boldsymbol{A}$, $\boldsymbol{B}$, $\boldsymbol{D}$, $\boldsymbol{E}$, $\boldsymbol{F}$, $\boldsymbol{G}$, and $\boldsymbol{H}$ are explicitly defined in Appendix A. Substituting (15) into (13) yields the desired form of the laminate strain energy given by

$$U = \frac{1}{2} \int_A \boldsymbol{e}^T \boldsymbol{C} \boldsymbol{e} \, dA. \tag{17}$$

As described in the preceding section, elastic extensional and rotational springs are employed to accommodate the enforcement of prescribed edge displacements ($\tilde{u}_x^*$, $\tilde{u}_y^*$, and $\tilde{u}_z^*$) and slopes ($\tilde{\vartheta}_x^*$ and $\tilde{\vartheta}_y^*$) defined in (6), along the boundary of the laminate, Γ_u. Associated with these displacements $\tilde{u}_x^*$, $\tilde{u}_y^*$, $\tilde{u}_z^*$ and with the slopes $\tilde{\vartheta}_x^*$, $\tilde{\vartheta}_y^*$ are the extensional and rotational spring stiffnesses S_x, S_y, S_z and $J_{\vartheta x}$, $J_{\vartheta y}$, respectively. As the concentrated loads P_x^* and P_y^* are applied to the rigid bar shown in Figure 1, the laminate undergoes the uniform edge displacements Δ_x and Δ_y. Associated with these uniform edge

displacements are the extensional spring stiffnesses, s_x and s_y. The potential energy that results from the elastic deformation of the springs, consistent with the {3, 0}-theory used herein, is given by

$$\Omega = \frac{1}{2} \int_{\Gamma_u} (\tilde{u} - \tilde{u}^*)^T k_u (\tilde{u} - \tilde{u}^*) \, d\Gamma + \frac{1}{2} \int_{\Gamma_\Delta} (\tilde{u} - \Delta)^T k_u (\tilde{u} - \Delta) \, d\Gamma, \tag{18}$$

where the vectors $\tilde{u}$, $\tilde{u}^*$, and Δ, and the matrices k_u and k_Δ, are defined as

$$\tilde{u}^T = \{\tilde{u}_x, \tilde{u}_y, \tilde{u}_z, \tilde{\vartheta}_x, \tilde{\vartheta}_y\}, \tag{19a}$$

$$\tilde{u}^{*T} = \{\tilde{u}_x^*, \tilde{u}_y^*, \tilde{u}_z^*, \tilde{\vartheta}_x^*, \tilde{\vartheta}_y^*\}, \tag{19b}$$

$$\Delta^T = \{\Delta_x, \Delta_y, 0, 0, 0\}, \tag{19c}$$

and

$$k_u = \begin{bmatrix} S_x & & & & \\ & S_y & & & \\ & & S_z & & \\ & & & J_{\vartheta x} & \\ & & & & J_{\vartheta y} \end{bmatrix}, \qquad k_\Delta = \begin{bmatrix} S_x & & & & \\ & S_y & & & \\ & & 0 & & \\ & & & 0 & \\ & & & & 0 \end{bmatrix}. \tag{19d}$$

The potential energy of the lateral pressure p^*, the external edge tractions (t_x^*, t_y^*, t_z^*), and the concentrated forces P_x^* and P_y^* acting on the rigid end-bar is given by

$$V = \int_{\Gamma_\sigma} \int_{-h/2}^{h/2} (t_x^* \tilde{U}_x + t_y^* \tilde{U}_y + t_z^* \tilde{U}_z) \, dz \, d\Gamma + \int_A p^* U_z \, dA + P_x^* \Delta_x + P_y^* \Delta_y. \tag{20}$$

Substituting (1), (2), and (5) into this expression and integrating through the thickness yields

$$V = \int_{\Gamma_\sigma} \left(N_x^* u_x + N_y^* u_y + N_z^* u_z - M_x^* \left(u_{z,x} - \frac{6}{5h} \Phi_{xz} \right) - M_y^* \left(u_{z,y} - \frac{6}{5h} \Phi_{yz} \right) \right) d\Gamma$$
$$+ \int_A p^* u_z \, dA + P_x^* \Delta_x + P_y^* \Delta_y, \tag{21a}$$

or

$$V = \int_{\Gamma_\sigma} T^{*T} \tilde{u} \, d\Gamma + \int_A p^* u_z \, dA + P^{*T} \Delta, \tag{21b}$$

in which the vector containing the resultant forces and moments acting along the boundary is given by

$$T^{*T} = \{N_x^*, N_y^*, N_z^*, -M_x^*, -M_y^*\}, \tag{22a}$$

and the prescribed point forces acting on the rigid end-bar are defined as

$$P^{*T} = \{P_x^*, P_y^*, 0, 0, 0\}. \tag{22b}$$

The explicit definitions of the stress and moment resultants (N_x^*, N_y^*, N_z^*) and (M_x^*, M_y^*) in (22) are given in Appendix A.

Equilibrium equations and boundary conditions. The nonlinear equilibrium equations and the corresponding boundary conditions are obtained by requiring the variation of the total potential energy of the laminate to vanish, that is,

$$\delta\pi = \delta U + \delta\Omega - \delta V = 0, \tag{23}$$

in which δU and $\delta\Omega$ represent the variation of strain energies of the laminate and the elastic edge supports (springs) due to the internal forces, and δV represents the variation of potential energy due to external boundary loads acting on the surface and around the boundary of the laminate. Their first variations are readily obtained from (17), (18), and (21) and are given explicitly in Appendix B. The resulting nonlinear partial differential equations and boundary conditions constitute a boundary-value problem that defines the stresses and displacements associated with stable and unstable deformation states in the realm of small strains and moderate rotations. The equations are applicable to laminates subjected to general loading conditions that exhibit anisotropy that couples all modes of deformation present in laminates with a general asymmetric lamination scheme. The equations needed to perform linear stress analysis can be obtained by direct linearization of the nonlinear plate equations. The specific form of these linearized equations is also given in Appendix B.

When a laminate is subjected to only in-plane loads, with monotonically increasing magnitudes, it may exhibit a flat stable equilibrium configuration for relatively small magnitudes of the loads. Then, a load level is reached at which a bent or buckled equilibrium configuration exists. This particular load level is obtained herein by linearizing the nonlinear plate equation with respect to the flat equilibrium configuration incipient to buckling [Brush and Almroth 1975]. The explicit forms of the resulting equations for buckling analyses are also given in Appendix B.

5. Solution method

Exact solutions for linear stress and buckling analyses of a composite laminate with a cutout are not mathematically tractable, especially when transverse shear deformations are included in the analyses. Therefore, a semianalytical approximate solution was constructed based on the principle of stationary potential energy.

In this approximate solution method, the midplane displacements $u_x(x, y)$, $u_y(x, y)$, and $u_z(x, y)$ and the higher-order in-plane deformation modes $\Phi_{xz}(x, y)$ and $\Phi_{yz}(x, y)$ are partitioned into global and local contributions. In particular,

$$u_i = \bar{u}_i + \bar{\bar{u}}_i \quad \text{with } i = x, y, z, \tag{24a}$$

and

$$\Phi_{iz} = \bar{\Phi}_{iz} + \bar{\bar{\Phi}}_{iz} \quad \text{with } i = x, y, \tag{24b}$$

where single and double overbars represent the global and local quantities, respectively. In the present formulation, no kinematic admissibility requirements on the local or global functions exist because of the presence of the elastic springs in the formulation. Robust, uniformly convergent Laurent series (used for doubly connected regions) are used for the local functions to enhance capturing steep stress gradients and deformations near a cutout, and complete sets of Chebyshev polynomials are used in series expansions primarily to capture the overall global response of the laminate. The global functions are defined to include all of the possible rigid-body modes associated with global translation and rotation

of the laminate. These rigid-body modes are eliminated in the analysis by enforcing the appropriate displacement boundary conditions. The Laurent series for the local quantities generally yield multivalued displacements. Therefore, single-valuedness of the local quantities must be enforced. This task is achieved by using Lagrange multipliers to enforce the required constraint conditions. The Lagrange multipliers can be viewed as the forces that are needed to enforce the corresponding constraints. The explicit form of the local and global quantities appearing in (24) and the constraint conditions are given in Appendix C.

In the solution method of the present study, the series expansions for the global and local quantities appearing in (24) are expressed in matrix form to yield

$$u_i = V_i^T q \qquad \text{with } i = x, y, z, \tag{25a}$$

$$\Phi_{iz} = V_{iz}^T q \qquad \text{with } i = x, y. \tag{25b}$$

In these expressions, the unknown coefficients of the local and global functions are arranged in the vector q, which is referred to herein as the vector of generalized coordinates. The explicit form for the vector of unknowns, q, and the known vector functions, V_i, are given in detail in Appendix C. Using (25), the total potential energy, π, of the laminate is expressed as

$$\pi(q, \Delta, \lambda) = U(q) + \Omega(q, \Delta) - V(q, \Delta) + W(q, \lambda), \tag{26}$$

in which U and Ω represent the strain energies of the laminate and the elastic edge supports (springs), and V represents the potential energy due to external boundary loads acting inside and around the boundary of the laminate. The vector Δ includes the unknown uniform edge-displacements that arise from the prescribed concentrated loads that are applied through the rigid end-bar. Because elastic edge supports are used as a means to relax the kinematic admissibility requirements on the assumed displacement functions, the potential energy of the constraint forces arising from the constraint equations must vanish. Therefore, the constraint equations are included in the total potential energy formulation by using Lagrange multipliers that produce zero potential energy; that is,

$$W(q, \lambda) = \lambda^T G_c q \equiv 0, \tag{27}$$

where W is the potential energy of constraint forces, G_c is the coefficient matrix of the constraint equations, and λ is a vector of Lagrange multipliers. The vector λ contains the unknown Lagrange multipliers of the constraint equations, and they represent the constraint forces. A detailed derivation is given in Appendix C.

Stress analysis. Under the presumption of infinitesimal displacement gradients, the potential energy is linearized by disregarding products of the displacement gradients. Thus, the vector of unknown generalized coordinates of the laminate, q, is associated only with the linear terms in the expression for total potential energy. The requirement that the first variation of the total potential vanish, $\delta\pi = 0$, yields the following equations for linear stress analysis:

$$\begin{bmatrix} K_{qq} + S_{qq} & G_c^T \\ G_c & 0 \end{bmatrix} \begin{Bmatrix} q \\ \lambda \end{Bmatrix} = \begin{Bmatrix} p_z^* + N^* - S_q^* \\ 0 \end{Bmatrix}, \tag{28}$$

in which the matrices $\boldsymbol{K}_{qq}$ and $\boldsymbol{S}_{qq}$ represent the stiffness of the laminate with a general stacking sequence and the stiffness of the springs associated with the deformation of the laminate, respectively. The vector $\boldsymbol{S}_q^*$ represents the loading that arises from displacements prescribed along the edges. The load vectors $\boldsymbol{N}^*$ and $\boldsymbol{p}_z^*$ are associated with the external tractions acting on the unrestrained edges of the laminate and the distributed loads acting over the surface of the laminate, respectively. The explicit forms of these matrices and vectors are given in Appendix D. Solving for the unknown vectors, $\boldsymbol{q}$ and $\boldsymbol{\lambda}$, in (28) permits the calculation of the displacements, strains, and stresses at any point of the laminate under general loading conditions.

Buckling analysis. As mentioned previously, the equations needed to perform buckling analyses are obtained by linearizing the nonlinear field equations about the known flat, stable, equilibrium configuration incipient to buckling. To simplify the linearization process, the vector of generalized coordinates $\boldsymbol{q}$, the uniform edge-displacement vector $\boldsymbol{\Delta}$, and the constraint force vector $\boldsymbol{\lambda}$ are combined into a single vector of unknowns, $\boldsymbol{Q}$, given by

$$\boldsymbol{Q}^T = \{\boldsymbol{q}^T, \boldsymbol{\Delta}^T, \boldsymbol{\lambda}^T\}. \tag{29}$$

As part of the linearization procedure, the vector $\boldsymbol{Q}$ is expressed as

$$\boldsymbol{Q} = \boldsymbol{Q}^{(0)} + e\,\boldsymbol{Q}^{(1)}, \tag{30}$$

where $\boldsymbol{Q}^{(0)}$ and $\boldsymbol{Q}^{(1)}$ correspond to the incipient prebuckling and adjacent equilibrium states, respectively, and e is a real number that can be made as small as required. The vector $\boldsymbol{Q}^{(0)}$ is obtained from a linear stress analysis and is presumed known in the buckling equations. Next, (30) is used to express the total potential energy in the form

$$\pi(\boldsymbol{Q}) = \pi^{(0)}(\boldsymbol{Q}^{(0)}) + e\pi^{(1)}(\boldsymbol{Q}^{(0)}, \boldsymbol{Q}^{(1)}) + e^2\pi^{(2)}(\boldsymbol{Q}^{(0)}, \boldsymbol{Q}^{(1)}) + O(e^3), \tag{31}$$

where $\pi^{(0)}$, $\pi^{(1)}$, and $\pi^{(2)}$ are functionals that are defined explicitly in Appendix E. The equations governing the prebuckling state incipient to buckling are obtained by enforcing

$$\delta\pi^{(0)} = 0, \tag{32a}$$

and the equations that define the load level for which an adjacent equilibrium state exists are obtained from

$$\delta\pi^{(2)} = 0, \tag{32b}$$

which is referred to as Treftz's criterion [Brush and Almroth 1975]. The boundary conditions associated with (32b) are homogeneous. Hence, the extensional and rotational springs are utilized only to apply fixed kinematic boundary conditions in the buckling analysis.

Enforcing the variational statement given by (32a) yields the matrix equation

$$\boldsymbol{K}\boldsymbol{Q}^{(0)} = \boldsymbol{F} \tag{33a}$$

for the prebuckling equilibrium states. The boundary conditions associated with (33a) are nonhomogeneous, so (33a) constitutes a well-posed linear boundary-value problem. In the solution of buckling problems, the applied loads are scaled proportionally by a loading parameter λ_c and, as a result, the

solution vector $\boldsymbol{Q}^{(0)}$ depends on the loading parameter. Thus, every prebuckling equilibrium state corresponds to a different value of λ_c. The relationship between the loading parameter, the relative proportions of the applied loads acting on a plate, and the solution vector $\boldsymbol{Q}^{(0)}$ can be expressed conveniently as

$$\boldsymbol{Q}^{(0)} = \lambda_c \overline{\boldsymbol{Q}}^{(0)}, \tag{33b}$$

where $\overline{\boldsymbol{Q}}^{(0)}$ represents a known prebuckling reference state. Similarly, enforcing the variational statement given by (32b) and using (33b) yields the matrix equation

$$\left[\boldsymbol{K} + \lambda_c \boldsymbol{H}(\overline{\boldsymbol{Q}}^{(0)}) \right] \boldsymbol{Q}^{(1)} = \boldsymbol{0}, \tag{33c}$$

which constitutes a linear generalized eigenvalue problem in which the loading parameter λ_c is the eigenvalue. The smallest positive value of λ_c represents the smallest load level at which the laminate has a nonflat adjacent equilibrium state in the shape of the corresponding eigenvector.

The matrices appearing in (33a) and (33c) are given by

$$\boldsymbol{K} = \begin{bmatrix} \boldsymbol{K}_{qq} & -\boldsymbol{s}_{q\Delta} & \boldsymbol{G}_c^T \\ -\boldsymbol{s}_{q\Delta}^T & \boldsymbol{s}_{\Delta\Delta} & \boldsymbol{0} \\ \boldsymbol{G}_c & \boldsymbol{0} & \boldsymbol{0} \end{bmatrix}, \qquad \boldsymbol{H}(\boldsymbol{Q}^{(0)}) = \begin{bmatrix} \boldsymbol{H}_s(\boldsymbol{Q}^{(0)}) & \boldsymbol{0} & \boldsymbol{0} \\ \boldsymbol{0} & \boldsymbol{0} & \boldsymbol{0} \\ \boldsymbol{0} & \boldsymbol{0} & \boldsymbol{0} \end{bmatrix}, \tag{34}$$

with

$$\boldsymbol{K}_{qq} = \boldsymbol{K}_C + \boldsymbol{S}_{qq}, \qquad \boldsymbol{F} = \begin{Bmatrix} \boldsymbol{N}^* \\ \boldsymbol{P}^* \\ \boldsymbol{0} \end{Bmatrix}. \tag{35}$$

The matrix $\boldsymbol{K}_C$ represents the stiffness of a symmetric laminate, as defined by (D7), and the matrix $\boldsymbol{S}_{qq}$ represents the stiffness of the springs associated with the deformation of the laminate, as defined in (D9a). The matrix $\boldsymbol{H}_S$, whose explicit form is given in Appendix E, is the stress-induced geometric stiffness of the laminate. The matrices $\boldsymbol{S}_{qq}$, $\boldsymbol{s}_{\Delta\Delta}$, and $\boldsymbol{s}_{q\Delta}$ represent the stiffness of the springs associated with the deformation of the laminate, the end-displacements, and their coupling, respectively. The derivation of these matrices is given in Appendix E. The load vectors $\boldsymbol{N}^*$ and $\boldsymbol{P}^*$ that appear in (35) are associated with the external tractions acting on the unrestrained edges of the laminate and the concentrated in-plane loads acting on the rigid end-bar, respectively. These vectors are defined as

$$\boldsymbol{N}^{*T} = \{N_x^*, N_y^*, 0, 0, 0, 0, 0\}, \qquad \boldsymbol{P}^{*T} = \{P_x^*, P_y^*, 0, 0, 0\}. \tag{36}$$

6. Numerical results

Results for two problems are presented in order to demonstrate the accuracy of the $\{3, 0\}$-plate theory for stress and buckling analyses. The first problem considered is the stress analysis of an angle-ply laminate with a centrally located circular cutout, subjected to a uniform lateral pressure load, as depicted in Figure 3 for a general rectangular laminate. The second problem considered is the buckling analysis of a square laminate that is subjected to uniform end-shortening and has a centrally located circular cutout. For both of these problems, the dimensions of the square laminate are given by $W = L = 10$ in and the cutout diameter is denoted by the symbol d. In addition, each ply is made of graphite-epoxy material with elastic lamina properties $E_{11} = 18.5 \times 10^6$ psi, $E_{22} = E_{33} = 1.6 \times 10^6$ psi, $G_{12} = G13 = 1.0 \times 10^6$ psi, $G_{23} = 0.64 \times 10^6$ psi, $v_{12} = v_{13} = 0.35$, and $v_{23} = 0.25$. Results are presented for several laminate

thickness-to-width ratios, h/W. As the value of this ratio changes, the ply thicknesses, t_k, are given by $t_k = h/20$.

Stress-analysis problem. For this problem, a square $[\pm\theta]_{5s}$ angle-ply laminate with a centrally located circular cutout is subjected to a uniform transverse pressure with a unit-magnitude intensity of $p_0 = 1$ psi, as depicted in Figure 3. The laminate is simply supported along the edges $x = 0$ and $x = W$, such that

$$\tilde{u}_z(x, y) = 0, \qquad \tilde{\vartheta}_y(x, y) = 0, \tag{37a}$$

and is clamped along the edges $y = 0$ and $y = W$, such that

$$\tilde{u}_x(x, y) = 0, \qquad \tilde{u}_y(x, y) = 0, \qquad \tilde{u}_z(x, y) = 0, \qquad \tilde{\vartheta}_x(x, y) = 0, \qquad \tilde{\vartheta}_y(x, y) = 0. \tag{37b}$$

Several results were obtained for this problem by using the analysis process of the present study. Corresponding results were also obtained from finite element analysis (FEA) based on the {1, 2}-plate theory of [Tessler and Saether 1991]. The finite element implementation of this theory was developed in [Tessler 1993] for linear analysis and extended to geometrically nonlinear analysis in [Barut et al. 1998]. The nonlinear element has three nodes with six degrees of freedom per node, and two additional element-dependent C^{-1} continuous fields that represent higher-order transverse displacement modes. As a result of a convergence study, the finite element model used consists of 6400 elements and 3360 nodes. In contrast, converged results were obtained with the present {3, 0}-plate theory by using Chebyshev polynomial series with 12 terms for the global displacement quantities and Laurent series with 6 terms for the local displacement quantities. The total number of unknowns in the solution vector, without the additional three constraint equations arising from the removal of the redundancy of the local kinematic field, is 575.

Critical in-plane stresses are expected to exist at the intersections of the cutout boundary with the cutout diameter that is parallel to the clamped edges. One of these points is labeled as A and located at the coordinates $(x, y, z) = (5 + d/2, 5, 0)$, where d is the cutout diameter. Similarly, critical transverse shear stresses are expected to occur at the midpoint of the straight laminate edges. These points are labeled B and C, and are located, respectively, at the coordinates $(10, 5, 0)$ and $(5, 10, 0)$. Therefore,
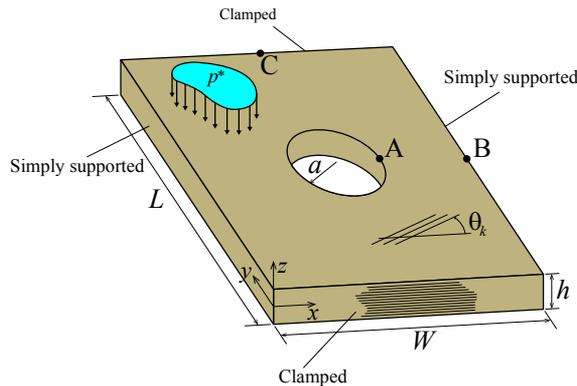
Figure 3. Square laminate with a central circular cutout, subjected to a uniform transverse pressure.

three points on the laminate midplane were selected for comparisons of selected stress variations obtained from the present analysis and the FEA.

Results are presented in Table 1 for $[\pm45]_{5s}$ laminates with a fixed thickness-to-width ratio given by $h/W = 0.1$. In particular, values of the out-of-plane displacement at the point $(x, y, z) = (5 + d/2, 5, 0)$ are given for select cutout sizes in the range $0.2 \leq d/W \leq 0.6$. These results indicate small differences between the displacements predicted by the two analyses that range from 0.47% to 1.65% as the cutout size increases from $d/W = 0.2$ to 0.6. Additional results are presented in Table 2 for the $[\pm45]_{5s}$ laminates with a fixed cutout size given by $d/W = 0.3$ and for select values of $0.05 \leq h/W \leq 0.2$. These results correspond to the point $(x, y, z) = (6.5, 5, 0)$ and also indicate small differences between the displacements predicted by the two analyses that range from 0.81% to 1.12% as the thickness-to-width ratio increases from $h/W = 0.05$ to 0.2. Similar results are presented in Table 3 for $[\pm\theta]_{5s}$

	u_z (in) $\times 10^5$		
d/W	Present: $\{3, 0\}$	FEA: $\{1, 2\}$	% Difference
0.2	4.25	4.23	0.47
0.3	3.86	3.84	0.52
0.4	3.23	3.21	0.62
0.5	2.52	2.49	1.19
0.6	1.82	1.79	1.65

Table 1. Out-of-plane displacement at $(x, y, z) = (5 + d/2, 5, 0)$ for $[\pm45°]_{5s}$ laminates with $h/W = 0.1$ as a function of cutout size d/W.

	u_z (in) $\times 10^5$)		
h/W	Present: $\{3, 0\}$	FEA: $\{1, 2\}$	% Difference
0.05	19.79	19.63	0.81
0.10	3.234	3.208	0.80
0.15	1.285	1.274	0.86
0.20	0.717	0.709	1.12

Table 2. Out-of-plane displacement at $(x, y, z) = (6.5, 5, 0)$ for $[\pm45°]_{5s}$ laminates with $d/W = 0.3$ as a function the thickness-to-width ratio h/W.

	u_z (in) $\times 10^5$)		
θ	Present: $\{3, 0\}$	FEA: $\{1, 2\}$	% Difference
0	8.243	8.200	0.52
30	4.144	4.099	1.09
60	2.905	2.879	0.90
90	3.085	3.070	0.49

Table 3. Out-of-plane displacement at $(x, y, z) = (6.5, 5, 0)$ for $[\theta/-\theta]_{5s}$ laminates with $d/W = 0.3$ and $h/W = 0.1$ as a function of the fiber angle θ.
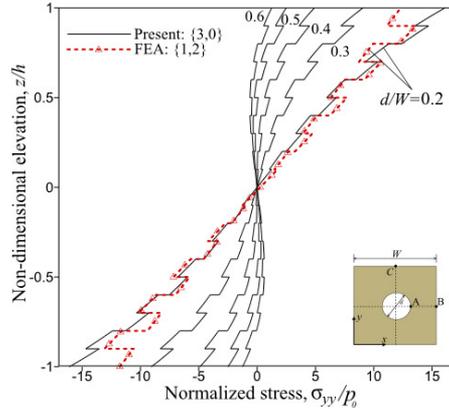
Figure 4. Effect of cutout size on the through-the-thickness variation of σ_{yy} at point A for a square $[\pm 45]_{5s}$ graphite-epoxy laminate with a central circular cutout, subjected to uniform pressure ($h/W = 0.1$).

laminates with a fixed thickness-to-width ratio given by $h/W = 0.1$ and a fixed cutout size given by $d/W = 0.3$. Specifically, results are given for select values of the ply orientation angle in the range $0 \leq \theta \leq 90$ degrees. These results also correspond to the point $(x, y, z) = (6.5, 5, 0)$ and indicate a very small effect of variations in the fiber angle.

Variations of through-the-thickness normal stress σ_{yy} at point A on the cutout edge, normalized by the magnitude of the applied pressure, are shown in Figure 4 for a $[\pm 45]_{5s}$ laminate with a thickness-to-width ratio of $h/W = 0.1$. Similarly, distributions of the normalized transverse shearing stresses σ_{xz} at point B on the simply supported edge and σ_{yz} at point C on the clamped edge are shown for this laminate in Figure 5. Several curves are shown in each figure for values of cutout diameter-to-width ratios given by $d/W = 0.2, 0.3, 0.4, 0.5$, and 0.6. The black solid lines correspond to results from the present analysis
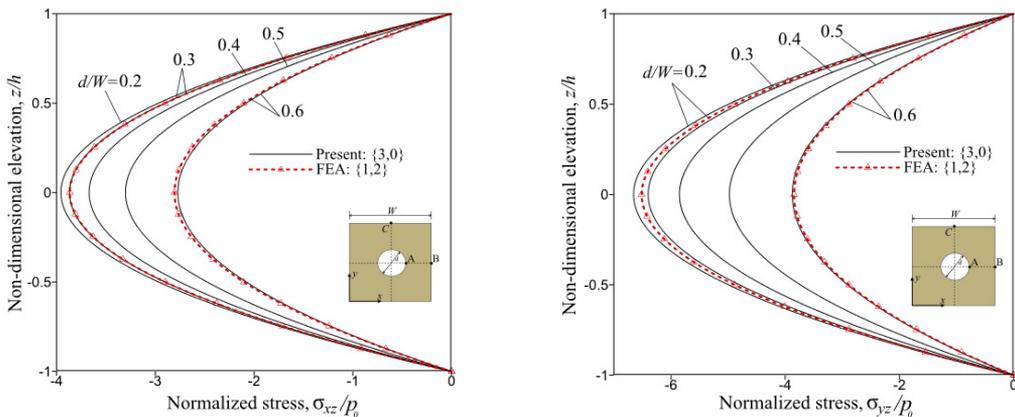
Figure 5. Effect of cutout size for a square $[\pm 45]_{5s}$ graphite-epoxy laminate with a central circular cutout, subjected to uniform pressure ($h/W = 0.1$). Left: through-the-thickness variation of σ_{xz} at point B (simply supported edge). Right: through-the-thickness variation of σ_{yz} at point C (clamped edge).
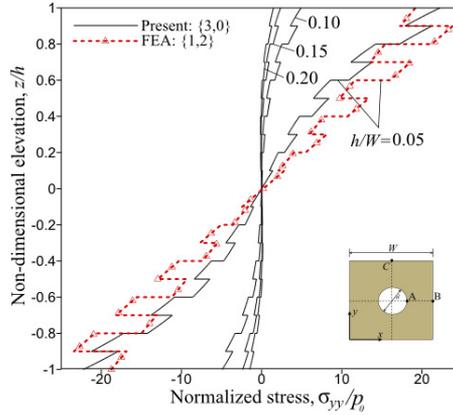
Figure 6. Effect of the plate thickness-to-width ratio on the through-the-thickness variation of σ_{yy} at point A for a square $[\pm 45]_{5s}$ graphite-epoxy laminate with a central circular cutout, subjected to uniform pressure ($d/W = 0.3$).

and the red dashed lines with triangular symbols correspond to results from the FEA. Discontinuities in the point-wise slope of the curves are associated with the piecewise constant lamina properties that are used to calculate stresses based on continuous through-the-thickness strain distributions.

The results in Figure 4 indicate that the present analysis yields a nonlinear variation σ_{yy/p_0} at point A whereas the finite-element solution based on the {1, 2}-plate theory yields a linear variation. Although results from the two analyses are only shown for $d/W = 0.2$, similar results were obtained for the other values of d/W that show the same trend. The maximum difference in the stresses predicted by the two theories is 26%, in contrast to the maximum difference in the corresponding out-of-plane displacements, which is less than 2%.

The results in Figure 5 indicate that the present analysis and the FEA yield identical through-the-thickness transverse shear stress distributions at points B and C, with slightly different amplitudes. The largest difference in the transverse shear stresses for the two plate theories is 2%. In these figures, the red dashed lines with triangular symbols (FEA) are shown only for the two extreme cases of $d/W = 0.2$ and 0.6, for clarity. Altogether, the results in Figures 4 and 5 indicate that the variation of the in-plane and transverse shear stresses diminishes with increasing cutout size. This trend is expected because increasing the hole size decreases the extent of loading surface and, as a result, reduces the net force applied to the laminate. Reducing the net applied force reduces the magnitude and through-the-thickness variation of all the stresses.

Variations of through-the-thickness normal stress σ_{yy} at point A on the cutout edge, normalized by the magnitude of the applied pressure, are shown in Figure 6 for a $[\pm 45]_{5s}$ laminate with a cutout diameter-to-width ratio $d/W = 0.3$. Similarly, distributions of the normalized transverse shearing stresses σ_{xz} at point B on the simply supported edge and σ_{yz} at point C on the clamped edge are shown for this laminate in Figure 7. Several curves are shown in each figure for values of thickness-to-width ratios of $h/W = 0.05, 0.10, 0.15$, and 0.20. The black solid lines correspond to results from the present analysis and the red dashed lines with triangular symbols correspond to results from the FEA. Discontinuities in the point-wise slope of these curves are also associated with the piecewise constant lamina properties that are used to calculate stresses based on continuous through-the-thickness strain distributions.
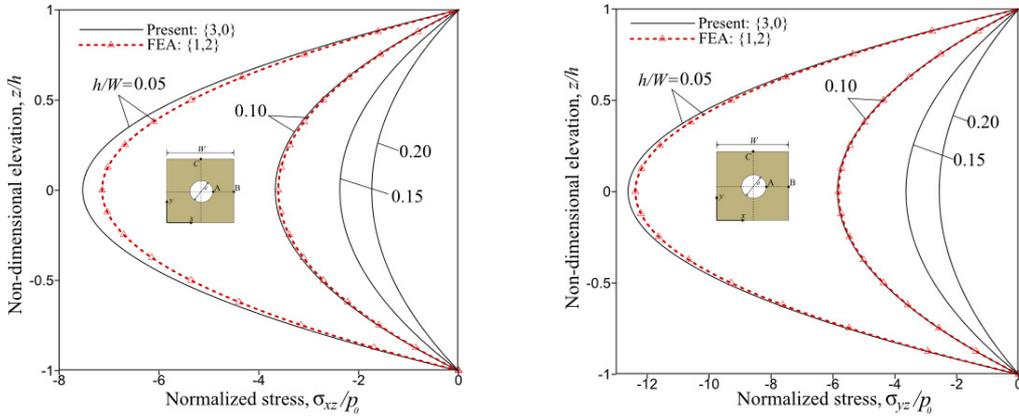
Figure 7. Effect of the plate thickness-to-width ratio for a square $[\pm45]_{5s}$ graphite-epoxy laminate with a central circular cutout, subjected to uniform pressure ($d/W = 0.3$). Left: through-the-thickness variation of σ_{xz} at point B (simply supported edge). Right: through-the-thickness variation of σ_{yz} at point C (clamped edge).

As expected, the results in Figure 6 also indicate that the present analysis yields a nonlinear variation σ_{yy}/p_0 at point A whereas the finite-element solution based on the {1, 2}-plate theory yields a linear variation. Although results from the two analyses are only shown for $h/W = 0.05$, similar results were obtained for the other values of h/W that show the same trend. Altogether, the maximum differences in the in-plane and transverse shear stresses predicted by the two theories for $h/W = 0.05$ and 0.1 are 29% and 4.8%, respectively. The results in Figures 6 and 7 also show an increase in stresses as h/W decreases. This increase in stresses is due to the reduction in bending stiffness with decreasing h/W and the fact that the laminate must carry the same applied load.

The effect of fiber angle, θ, on through-the-thickness variation σ_{yy} at point A located on the cutout edge is shown for $[\pm\theta]_{5s}$ laminates with $d/W = 0.3$ and $h/W = 0.1$ in Figure 8. The corresponding
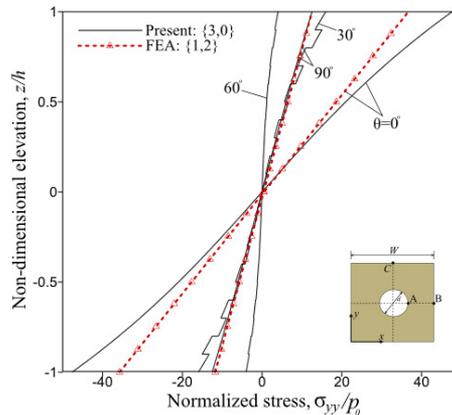
Figure 8. Effect of fiber angle on the through-the-thickness variation of σ_{yy} at point A for a square $[\pm\theta]_{5s}$ graphite-epoxy laminate with a central circular cutout, subjected to uniform pressure ($d/W = 0.3$, $h/W = 0.1$).
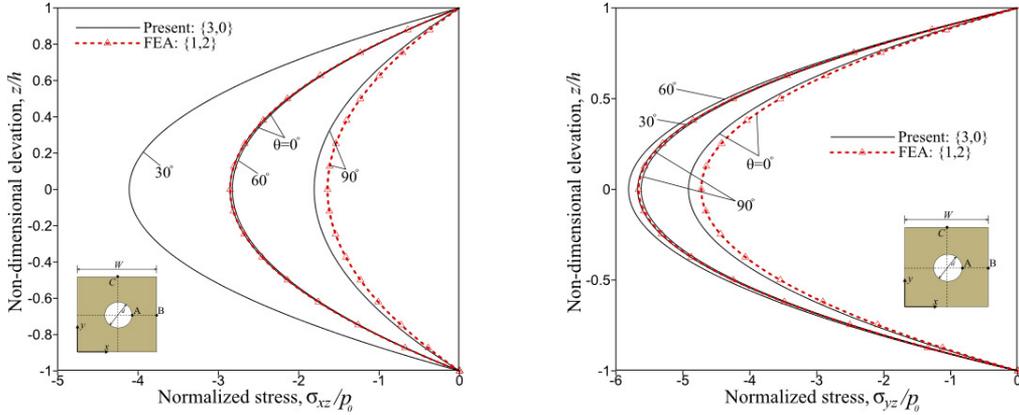
Figure 9. Effect of fiber angle for a $[\pm\theta]_{5s}$ graphite-epoxy laminate with a central circular cutout, subjected to uniform pressure ($d/W = 0.3$, $h/W = 0.1$). Left: through-the-thickness variation of σ_{xz} at point B (simply supported edge). Right: through-the-thickness variation of σ_{yz} at point C (clamped edge).

distributions of the normalized transverse shearing stresses σ_{xz} at point B (on the simply supported edge) and σ_{yz} at point C (on the clamped edge) are shown for this laminate in Figure 9. Several curves are shown in each figure for values of $\theta = 0, 30, 60,$ and 90 degrees. The black solid lines correspond to results from the present analysis and the red dashed lines with triangular symbols for $\theta = 0$ and 90 degrees correspond to results from the FEA. Discontinuities in the point-wise slope of these curves are also associated with the piecewise constant lamina properties that are used to calculate stresses based on continuous through-the-thickness strain distributions.

The results in Figure 8 show that the largest variation in the in-plane stress σ_{yy} occurs for $\theta = 0$ degrees. Similarly, the results in Figure 9 show the largest variations in σ_{xz} and σ_{yz} for $\theta = 30$ and 60 degrees, respectively. The results in Figure 8 also show better agreement in predicted values of σ_{yy} at point A obtained from the two theories for $\theta = 90$ degrees than for $\theta = 0$ degrees. Likewise, the results in Figure 9, right, show better agreement in predicted values of σ_{yz} at point C for $\theta = 90$ degrees than for $\theta = 0$ degrees. In contrast, the results in Figure 9, left, show better agreement in predicted values of σ_{xz} at point B for $\theta = 0$ degrees than for $\theta = 90$ degrees.

Buckling-analysis problem. The second problem considered is buckling of a square $[+\theta_5/-\theta_5]_s$ laminate with a central circular cutout, subjected to uniform end-shortening, as shown in Figure 10. This pathological family of laminates was chosen because of the high degree of anisotropy that exists in the form of coupling between pure-bending and twisting deformations. The dimensions of this square laminate are also given by $W = L = 10$ in and the diameter of the cutout is specified as $d = 6$ in. The values of the thickness-to-width ratios considered for this problem are $h/W \leq 0.05$, and were chosen such that elastic buckling is likely to occur prior to a first-ply failure. This range of h/W values was determined by using the point-stress failure criteria of [Whitney and Nuismer 1974] with a critical strength value of $X = 320$ ksi. Two sets of boundary conditions are also considered. Specifically, the edges at $x = 0$ and $x = W$ are simply supported, and those at $y = 0$ and $y = L$ are either simply supported or clamped.
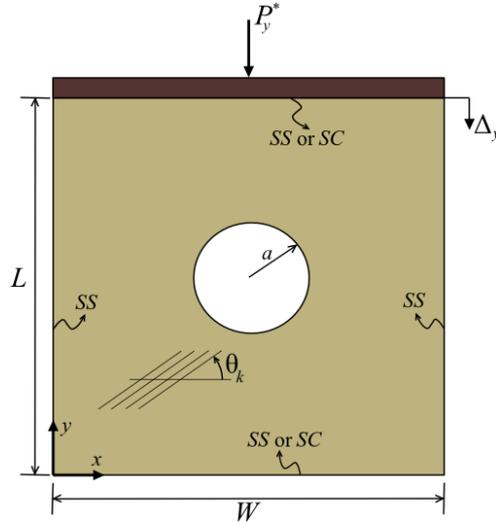
Figure 10. Square laminate with a circular cutout, subjected to uniform end-shortening.

The load is introduced into the laminate as a uniform end-shortening, Δ_y, that results from applying the concentrated force $-P_y^*$ to a rigid end-bar. In addition, the unloaded lateral edges are free to expand and contract. In particular, the two sets of boundary are specified and designated as follows.

- Two simply supported and two clamped opposite edges (SS-CL):

$$\tilde{u}_z = \tilde{\vartheta}_y = 0 \qquad\qquad \text{at } x = 0 \text{ and } x = W, \qquad (38a)$$

$$\tilde{u}_y = \tilde{u}_z = \tilde{\vartheta}_x = \tilde{\vartheta}_y = 0 \qquad\qquad \text{at } y = 0, \qquad (38b)$$

$$\tilde{u}_z = \tilde{\vartheta}_x = \tilde{\vartheta}_y = 0 \text{ and } \tilde{u}_y = \Delta_y \text{ through } -P_y^* \qquad \text{at } y = L. \qquad (38c)$$

- All edges simply supported (SS-SS):

$$\tilde{u}_z = \tilde{\vartheta}_y = 0 \qquad\qquad \text{at } x = 0 \text{ and } x = W, \qquad (39a)$$

$$\tilde{u}_y = \tilde{u}_z = \tilde{\vartheta}_x = 0 \qquad\qquad \text{at } y = 0, \qquad (39b)$$

$$\tilde{u}_z = \tilde{\vartheta}_x = 0 \text{ and } \tilde{u}_y = \Delta_y \text{ through } -P_y^* \qquad \text{at } y = L. \qquad (39c)$$

Several buckling predictions obtained by using the present analysis were compared with corresponding results obtained from the FEA based on a {1, 2}-order plate theory developed in [Barut et al. 1998]. In these analyses, converged solutions were obtained by using the finite element model with 6400 elements and 3360 nodes that was used in the stress analyses. Likewise, 12-term Chebyshev polynomial series and 6-term Laurent series were used in the present analysis. In addition, corresponding results were also obtained by using the semianalytical method developed in [Barut and Madenci 2001], which is based on classical laminated plate theory (CLPT) and formulated in a manner similar to the present analysis.

The buckling loads obtained by using the three analysis methods are presented in Tables 4 and 5 for $[+\theta_5/-\theta_5]_s$ laminates with $h/W = 0.035$ and $d/W = 0.6$. The results in Tables 4 and 5 are for laminates with SS-CL and SS-SS boundary conditions, respectively, and are given for select values of the fiber angle
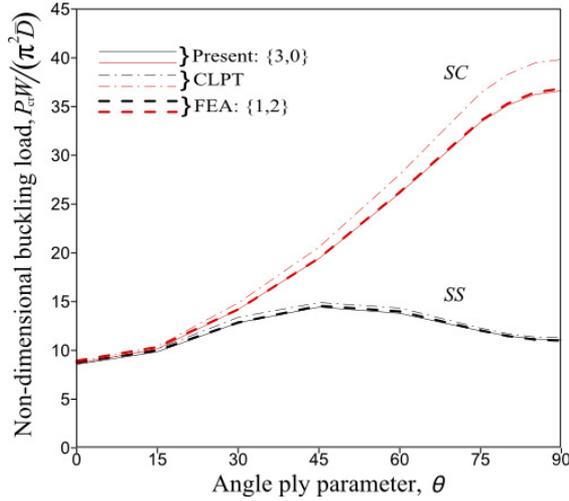
Figure 11. Effects of boundary conditions and transverse shear flexibility on the buckling resistance of $[+\theta_5/-\theta_5]_s$ angle-ply laminates with a central circular cutout, subjected to uniform end-shortening ($h/W = 0.035$, $d/W = 0.6$).

θ. These results are also shown in Figure 11, where the buckling load is given in nondimensional form as $P_{cr}W/(\pi^2\bar{D})$, and where $\bar{D}$ denotes the bending stiffness defined as $\bar{D} = E_T h^3/[12(1 - v_{LT}^2)]$ and P_{cr} is the value of the applied load at buckling. The results obtained from the present analysis are represented by the solid lines in the figures, FEA results are represented by the thick-dashed lines, and results based on CLPT are represented by the dash-dotted lines. Also, the red and black lines correspond to results for the SS-CL and SS-SS boundary conditions, respectively.

The results in these tables and in Figure 11 show very good agreement between the present analysis and the FEA. For all values of θ the differences in the buckling loads predicted by the two shear-deformation-based theories are less than 3%. The results also indicate maximum differences between the buckling loads obtained by using the present analysis and the CLPT analysis of approximately 6% and 9% for the

Fiber angle, θ (deg)	Buckling load (kips)		
	Present: {3, 0}	FEA: {1, 2}	CLPT
0	55.646	57.463	56.504
15	73.762	75.043	75.892
30	114.532	114.000	121.201
45	156.650	156.490	167.471
60	198.143	199.574	213.171
75	228.638	230.546	246.813
90	235.416	236.930	256.077

Table 4. Buckling loads of $[+\theta_5/-\theta_5]_s$ angle-ply laminates with a central circular cutout, subjected to uniform end-shortening, with SS-CL boundary conditions ($h/W = 0.035$, $d/W = 0.6$).
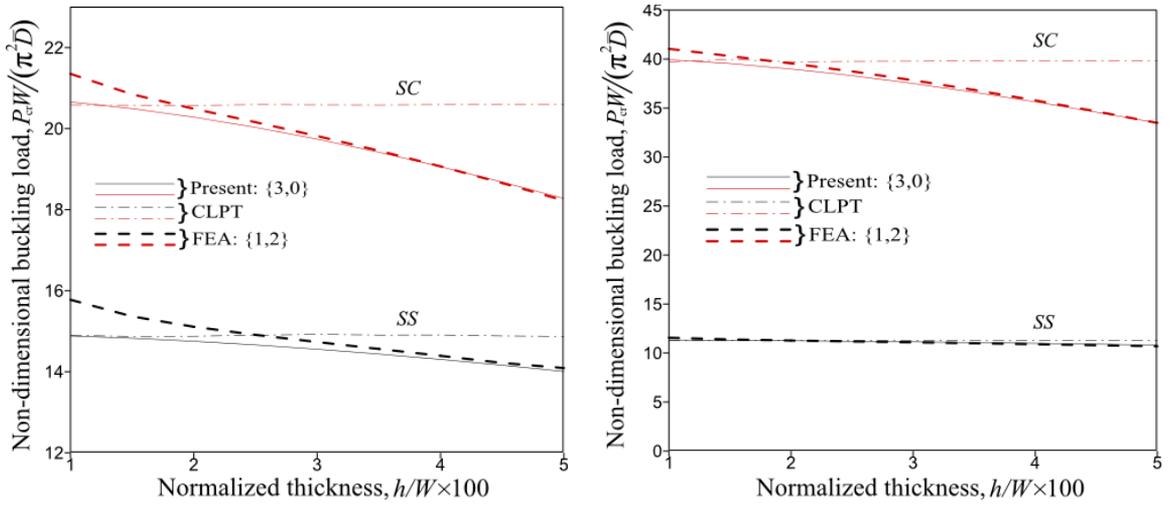
Figure 12. Effect of thickness-to-width ratio and transverse shear flexibility on the buckling resistance of angle-ply laminates with a central circular cutout, subjected to uniform end-shortening ($d/W = 0.6$). Left: $[+45_5^\circ/-45_5^\circ]_s$ laminate. Right: $[90^\circ]_{20}$ unidirectional laminate.

laminates with SS-SS and SS-CL boundary conditions, respectively. Moreover, the maximum difference occurred for $\theta = 30$ and 90 degrees for the laminates with SS-SS and SS-CL boundary conditions, respectively. The results in Figure 11 also indicate that the boundary conditions influence the importance of transverse shear flexibility in addition to how fiber angle affects buckling resistance.

The effects of the thickness-to-width ratio h/W on the buckling predictions for $[+\theta_5/-\theta_5]_s$ angle-ply laminates with $d/W = 0.6$ are shown in Figure 12 for $\theta = 45$ and 90 degrees. Laminates with $\theta = 45$ degrees have a very high degree of anisotropy in the form of coupling between pure-bending and twisting deformations. In contrast, laminates with $\theta = 90$ degrees are unidirectional, aligned with the loading direction, and have a very high degree of orthotropy. Two groups of curves, one red and one

	Buckling load (kips)		
Fiber angle, θ (deg)	Present: {3, 0}	FEA: {1, 2}	CLPT
0	55.012	56.270	55.523
15	63.399	64.226	65.254
30	82.521	82.667	86.091
45	92.826	93.636	96.268
60	88.736	89.926	92.261
75	77.121	77.438	78.997
90	71.160	70.701	72.464

Table 5. Buckling loads of $[+\theta_5/-\theta_5]_s$ angle-ply laminates with a central circular cutout, subjected to uniform end-shortening, with SS-SS boundary conditions ($h/W = 0.035$, $d/W = 0.6$).

black, are shown in each figure, corresponding to laminates with SS-SS and SS-CL boundary conditions, respectively. In each group of curves, the solid lines correspond to results obtained with the present analysis, while thick dashed and dash-dotted lines correspond to results obtained from the CLPT-based analysis and the FEA, respectively.

The results in Figure 12, left, for $\theta = 45$ degrees, generally show discrepancies between the results obtained by using all three analysis methods that are more pronounced for the SS-CL than for the SS-SS boundary condition. For the thinner laminates, the results obtained from the present analysis and the CLPT-based analysis are in very good agreement, but neither set of results agrees with the corresponding results obtained by using the FEA. For the thinner laminates, the FEA overpredicts the buckling loads. As the laminate thickness increases, the agreement between the results obtained from the present analysis and the FEA becomes very good, but neither set of results agrees with the corresponding results obtained by using the CLPT-based analysis. In addition, the CLPT results significantly overpredict the buckling loads for the larger values of h/W. In particular, the largest difference in the results obtained from the CLPT-based analysis and the two shear-deformation-based analyses is 11% for the SS-SS laminates and 5% in the case of SS-CL laminates, for the upper limit of $h/W = 0.05$ shown in the figure. The results in Figure 12, right, for $\theta = 90$ degrees, show the same trends for the SS-CL laminates; however, the results for the SS-SS laminates obtained from the three analysis methods are in very good agreement. The largest differences in the results obtained from the CLPT-based analysis and the two shear-deformation-based analyses are 15% for the SS-SS laminates and less than 2% in the case of SS-CL laminates, for the upper limit of $h/W = 0.05$ shown in Figure 12, left.

Typical buckling modes are shown in Figures 13 and 14 for the laminates with $\theta = 45$ and 90 degrees, respectively, and with $h/W = 0.035$ and $d/W = 0.6$. Two modes are shown in each figure that correspond to the SS-CL and SS-SS boundary conditions. The mode shapes shown in Figure 13 for the laminates with
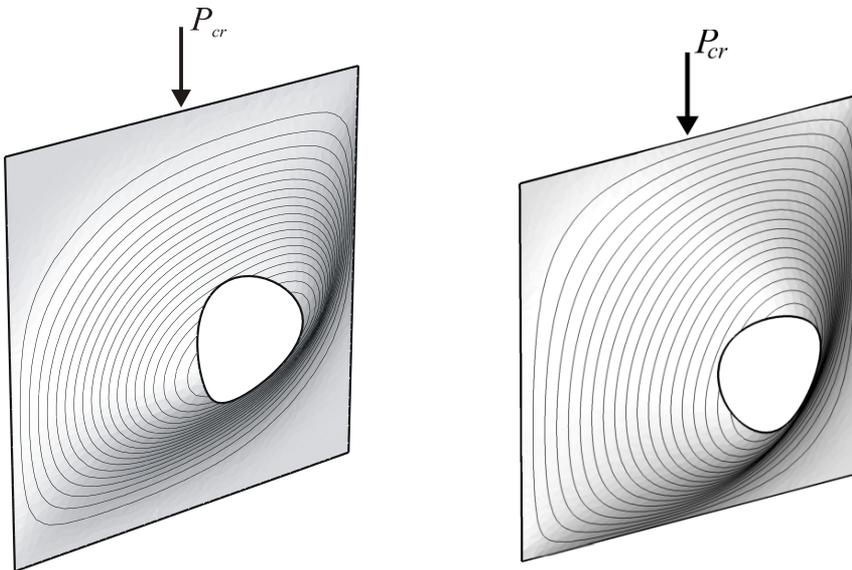
Figure 13. Buckling modes for a $[45_5^\circ/-45_5^\circ]_s$ laminate with $h/W = 0.035$ and $d/W = 0.6$: (a) SS-CL and (b) SS-SS boundary conditions.
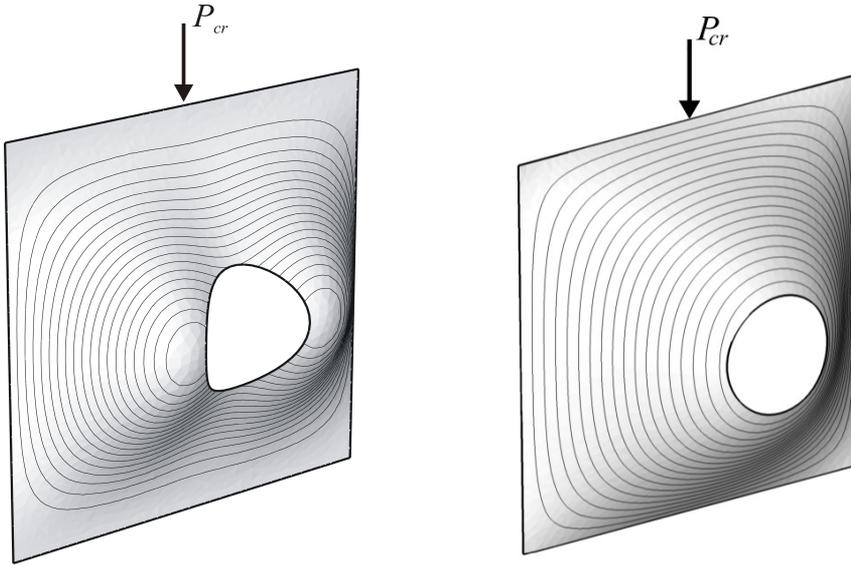
Figure 14. Buckling modes for a $[90°]_{20}$ laminate with $h/W = 0.035$ and $d/W = 0.6$: (a) SC and (b) SS-type boundary conditions.

$\theta = 45$ degrees are skewed for both boundary-condition cases, as a result of the high degree of bending-twisting anisotropy. In addition, the buckle pattern for the SS-CL boundary condition (Figure 13a) is flatter than that for the SS-SS boundary condition (Figure 13b), as expected. The buckle patterns shown in Figure 14 for the laminates with $\theta = 90$ degrees exhibit bilateral symmetry for both sets of boundary conditions. However, the buckle pattern for the unidirectional laminate with the clamped loaded edges exhibits three half waves in the horizontal x-direction (weak direction), as shown in Figure 14a, as compared to one half wave for the SS-SS laminate shown in Figure 14b. The buckling mode shown in Figure 14a for the SS-CL boundary conditions has the same features as the experimentally determined buckle pattern of a similar specially orthotropic plate that was presented in [Nemeth 1990].

7. Conclusions

A semianalytical solution method for predicting the bending and buckling behavior of a moderately thick laminate with a cutout has been presented. The analysis method has been validated for linear stress analyses of laminates with a cutout and subjected to uniform lateral pressure against corresponding results obtained from finite element analyses (FEA) based on a {1, 2} shear deformation plate theory appearing in the literature. The agreement between the present method and the FEA was found to be excellent. In all cases considered, the maximum difference in the out-of-plane displacements predicted by the two methods is less than 2%. Comparisons of the through-the-thickness stress variations also showed favorable agreement between the two approaches, despite the fact that the FEA are based on a plate theory that cannot capture nonuniform through-the-thickness variations of the in-plane stresses for thick plates.

The present method has also been validated for the buckling analyses of pathological highly orthotropic and highly anisotropic laminates with relatively large cutouts, subjected to uniform end-shortening. Comparisons of results obtained by the present method with the corresponding results obtained from the FEA and from a similar semianalytical solution method based on CLPT have been presented for two sets of boundary conditions. The comparisons with the FEA show close agreement between the two shear-deformation-based analyses, for the most part. Differences were found for relatively small values of the thickness-to-width ratio, h/W. In contrast, very good agreement between the present analysis and the FEA was found for the larger values of h/W. Results have also been presented that show the effects of laminate orthotropy and anisotropy, and boundary conditions, on the importance of including transverse shear flexibility in the analysis. Overall, the analysis method presented herein successfully captures the effects of transverse shear flexibility and represents boundary conditions adequately, which is problematic for some analyses based on a transverse shear deformation theory.

Appendix A: Stress resultants and constitutive equations

The stress resultants appearing in (12) are defined as

$$\begin{Bmatrix} N_{xx} \\ N_{yy} \\ N_{xy} \end{Bmatrix} = \int_{-h/2}^{+h/2} \begin{Bmatrix} \sigma_{xx} \\ \sigma_{yy} \\ \sigma_{xy} \end{Bmatrix} dz, \qquad \begin{Bmatrix} M_{xx} \\ M_{yy} \\ M_{xy} \end{Bmatrix} = \int_{-h/2}^{+h/2} \begin{Bmatrix} \sigma_{xx} \\ \sigma_{yy} \\ \sigma_{xy} \end{Bmatrix} z \, dz, \qquad \text{(A1a)}$$

$$\begin{Bmatrix} F_{xx} \\ F_{yy} \\ F_{xy} \end{Bmatrix} = \int_{-h/2}^{+h/2} \begin{Bmatrix} \sigma_{xx} \\ \sigma_{yy} \\ \sigma_{xy} \end{Bmatrix} \Lambda(z) \, dz, \qquad \begin{Bmatrix} q_{xz} \\ q_{yz} \end{Bmatrix} = \int_{-h/2}^{+h/2} \begin{Bmatrix} \sigma_{xz} \\ \sigma_{yz} \end{Bmatrix} \Lambda'(z) \, dz, \qquad \text{(A1b)}$$

where h is the plate thickness. In terms of the notation used in [Ray 2003],

$$\begin{Bmatrix} F_{xx} \\ F_{yy} \\ F_{xy} \end{Bmatrix} = \frac{3}{2h} \left(\begin{Bmatrix} M_{xx} \\ M_{yy} \\ M_{xy} \end{Bmatrix} - \frac{4}{3h^2} \begin{Bmatrix} P_{xx} \\ P_{yy} \\ P_{xy} \end{Bmatrix} \right), \qquad \begin{Bmatrix} f_{xz} \\ f_{yz} \end{Bmatrix} = \frac{3}{2h} \left(\begin{Bmatrix} Q_x \\ Q_y \end{Bmatrix} - \frac{4}{h^2} \begin{Bmatrix} R_x \\ R_y \end{Bmatrix} \right), \qquad \text{(A1c)}$$

where Q_x and Q_y are the transverse shear stress resultants of CLPT given by

$$\begin{Bmatrix} Q_{xz} \\ Q_{yz} \end{Bmatrix} = \int_{-h/2}^{+h/2} \begin{Bmatrix} \sigma_{xz} \\ \sigma_{yz} \end{Bmatrix} dz, \qquad \text{(A2a)}$$

and

$$\begin{Bmatrix} P_{xx} \\ P_{yy} \\ P_{xy} \end{Bmatrix} = \int_{-h/2}^{+h/2} \begin{Bmatrix} \sigma_{xx} \\ \sigma_{yy} \\ \sigma_{xy} \end{Bmatrix} z^3 \, dz, \qquad \begin{Bmatrix} R_x \\ R_y \end{Bmatrix} = \int_{-h/2}^{+h/2} \begin{Bmatrix} \sigma_{xz} \\ \sigma_{yz} \end{Bmatrix} z^2 \, dz. \qquad \text{(A2b)}$$

The constitutive equations used in the present theory are those for a plate made of one or more layers of linear elastic, specially orthotropic materials. As a result, the plate is generally inhomogeneous through the thickness. These equations, referred to the corresponding (x, y, z) plate coordinate system, are given

by

$$\begin{Bmatrix} \sigma_{xx} \\ \sigma_{yy} \\ \sigma_{xy} \end{Bmatrix} = \begin{bmatrix} \bar{Q}_{11} & \bar{Q}_{12} & \bar{Q}_{16} \\ \bar{Q}_{12} & \bar{Q}_{22} & \bar{Q}_{26} \\ \bar{Q}_{16} & \bar{Q}_{26} & \bar{Q}_{66} \end{bmatrix} \begin{Bmatrix} \epsilon_{xx} \\ \epsilon_{yy} \\ \gamma_{xy} \end{Bmatrix}, \qquad \begin{Bmatrix} \sigma_{yz} \\ \sigma_{xz} \end{Bmatrix} = \begin{bmatrix} \bar{C}_{44} & \bar{C}_{45} \\ \bar{C}_{45} & \bar{C}_{55} \end{bmatrix} \begin{Bmatrix} \gamma_{yz} \\ \gamma_{xz} \end{Bmatrix}, \tag{A3}$$

where the subscripted σ_{ij} with $i, j = x, y, z$ are the stress components, $\bar{Q}_{ij} = \bar{Q}_{ij}(z)$ are the transformed, reduced stiffness matrix coefficients of CLPT, and $\bar{C}_{ij} = \bar{C}_{ij}(z)$ are the transformed transverse shearing stiffnesses of the FSDT [Jones 1975]. These equations reveal that, if the transverse shearing strains vanish on the bounding surfaces of a plate, the transverse shearing stresses also vanish on the bounding surfaces of the plate.

The submatrices in (16) are defined as

$$\mathbf{A} = \begin{bmatrix} A_{11} & A_{12} & A_{16} \\ A_{12} & A_{22} & A_{26} \\ A_{16} & A_{26} & A_{66} \end{bmatrix} = \int_{-h/2}^{+h/2} \begin{bmatrix} \bar{Q}_{11} & \bar{Q}_{12} & \bar{Q}_{16} \\ \bar{Q}_{12} & \bar{Q}_{22} & \bar{Q}_{26} \\ \bar{Q}_{16} & \bar{Q}_{26} & \bar{Q}_{66} \end{bmatrix} dz, \tag{A4a}$$

$$\mathbf{B} = \begin{bmatrix} B_{11} & B_{12} & B_{16} \\ B_{12} & B_{22} & B_{26} \\ B_{16} & B_{26} & B_{66} \end{bmatrix} = \int_{-h/2}^{+h/2} \begin{bmatrix} \bar{Q}_{11} & \bar{Q}_{12} & \bar{Q}_{16} \\ \bar{Q}_{12} & \bar{Q}_{22} & \bar{Q}_{26} \\ \bar{Q}_{16} & \bar{Q}_{26} & \bar{Q}_{66} \end{bmatrix} z \, dz, \tag{A4b}$$

$$\mathbf{D} = \begin{bmatrix} D_{11} & D_{12} & D_{16} \\ D_{12} & D_{22} & D_{26} \\ D_{16} & D_{26} & D_{66} \end{bmatrix} = \int_{-h/2}^{+h/2} \begin{bmatrix} \bar{Q}_{11} & \bar{Q}_{12} & \bar{Q}_{16} \\ \bar{Q}_{12} & \bar{Q}_{22} & \bar{Q}_{26} \\ \bar{Q}_{16} & \bar{Q}_{26} & \bar{Q}_{66} \end{bmatrix} z^2 \, dz, \tag{A4c}$$

$$\mathbf{E} = \begin{bmatrix} E_{11} & E_{12} & E_{16} \\ E_{12} & E_{22} & E_{26} \\ E_{16} & E_{26} & E_{66} \end{bmatrix} = \int_{-h/2}^{+h/2} \begin{bmatrix} \bar{Q}_{11} & \bar{Q}_{12} & \bar{Q}_{16} \\ \bar{Q}_{12} & \bar{Q}_{22} & \bar{Q}_{26} \\ \bar{Q}_{16} & \bar{Q}_{26} & \bar{Q}_{66} \end{bmatrix} \Lambda(z) \, dz, \tag{A4d}$$

$$\mathbf{F} = \begin{bmatrix} F_{11} & F_{12} & F_{16} \\ F_{12} & F_{22} & F_{26} \\ F_{16} & F_{26} & F_{66} \end{bmatrix} = \int_{-h/2}^{+h/2} \begin{bmatrix} \bar{Q}_{11} & \bar{Q}_{12} & \bar{Q}_{16} \\ \bar{Q}_{12} & \bar{Q}_{22} & \bar{Q}_{26} \\ \bar{Q}_{16} & \bar{Q}_{26} & \bar{Q}_{66} \end{bmatrix} \Lambda(z) z \, dz, \tag{A4e}$$

$$\mathbf{H} = \begin{bmatrix} H_{11} & H_{12} & H_{16} \\ H_{12} & H_{22} & H_{26} \\ H_{16} & H_{26} & H_{66} \end{bmatrix} = \int_{-h/2}^{+h/2} \begin{bmatrix} \bar{Q}_{11} & \bar{Q}_{12} & \bar{Q}_{16} \\ \bar{Q}_{12} & \bar{Q}_{22} & \bar{Q}_{26} \\ \bar{Q}_{16} & \bar{Q}_{26} & \bar{Q}_{66} \end{bmatrix} (\Lambda(z))^2 \, dz, \tag{A4f}$$

$$\mathbf{G} = \begin{bmatrix} G_{55} & G_{45} \\ G_{45} & G_{44} \end{bmatrix} = \int_{-h/2}^{+h/2} \begin{bmatrix} \bar{C}_{55} & \bar{C}_{45} \\ \bar{C}_{45} & \bar{C}_{44} \end{bmatrix} (\Lambda'(z))^2 \, dz. \tag{A4g}$$

Substituting the strain expressions given by (7a) and (7b) into the stresses given by (A3) and performing the through-the-thickness integrations in (A1) yields the laminate constitutive equations as

$$\mathbf{N} = \mathbf{A}\boldsymbol{\epsilon}^0 + \mathbf{B}\boldsymbol{\kappa}^0 + \mathbf{E}\boldsymbol{\Gamma}^0, \qquad \mathbf{M} = \mathbf{B}\boldsymbol{\epsilon}^0 + \mathbf{D}\boldsymbol{\kappa}^0 + \mathbf{F}\boldsymbol{\Gamma}^0, \qquad \mathbf{F} = \mathbf{E}\boldsymbol{\epsilon}^0 + \mathbf{F}\boldsymbol{\kappa}^0 + \mathbf{H}\boldsymbol{\Gamma}^0, \tag{A5a}$$

$$\mathbf{f} = \mathbf{G}\boldsymbol{\Phi}. \tag{A5b}$$

For the laminated plates investigated in [Ray 2003], the expression

$$\Lambda(z) = \tfrac{3}{2}(z/h) - 2(z/h)^3 \tag{A6}$$

was used to obtain the laminate constitutive equations given by (A5a). In particular, using (A6) with (A5a) the constitutive equations reduce to

$$\mathbf{N} = \mathbf{A}\boldsymbol{\epsilon}^0, \qquad \mathbf{M} = \mathbf{D}\boldsymbol{\kappa}^0 + \mathbf{F}\boldsymbol{\Gamma}^0, \qquad \mathbf{F} = \mathbf{F}\boldsymbol{\kappa}^0 + \mathbf{H}\boldsymbol{\Gamma}^0, \tag{A7}$$

for symmetrically laminated plates. The first of these equations indicates that there is no coupling between membrane action and bending or transverse shearing actions. In contrast, the last two parts of (A7) indicate strong coupling between bending and/or transverse shearing actions.

The resultant forces and moments appearing in (22) that are associated with the applied edge tractions are defined as

$$N_x^* = \int_{-h/2}^{h/2} t_x^* \, dz, \qquad N_y^* = \int_{-h/2}^{h/2} t_y^* \, dz, \qquad N_z^* = \int_{-h/2}^{h/2} t_z^* \, dz, \tag{A8a}$$

$$M_x^* = \int_{-h/2}^{h/2} z t_x^* \, dz, \qquad M_y^* = \int_{-h/2}^{h/2} z t_y^* \, dz. \tag{A8b}$$

Appendix B: Nonlinear and linearized forms of equations for stress and buckling analyses

The first variations of the strain energies of the laminate, the elastic edge supports (springs) due to the internal forces, and the potential energy due to external boundary loads acting on the surface and around the boundary of the laminate, δU, $\delta \Omega$, and δV, respectively, are derived in the form

$$
\begin{aligned}
\delta U = -\int_A \Big\{ & (N_{xx,x} + N_{xy,y})\delta u_x + (N_{yy,y} + N_{xy,x})\delta u_y \\
& + \big(M_{xx,xx} + 2M_{xy,xy} + M_{yy,yy} + [N_{xx}u_{z,x} + N_{xy}u_{z,y}]_{,x} + [N_{yy}u_{z,y} + N_{xy}u_{z,x}]_{,y}\big)\delta u_z \\
& + (F_{xx,x} + F_{xy,y} - q_{xz})\delta\Phi_{xz} + (F_{yy,y} + F_{xy,y} - q_{yz})\delta\Phi_{yz} \Big\} \, dA \\
& + \int_\Gamma \Big\{ (N_{xx}n_x + N_{xy}n_y)\delta u_x + (N_{yy}n_y + N_{xy}n_x)\delta u_y \\
& + \big(M_{xx,x}n_x + M_{yy,y}n_y + M_{xy,y}n_x + M_{xy,x}n_y + N_{xx}u_{z,x}n_x + N_{yy}u_{z,y}n_y + N_{xy}u_{z,x}n_y + N_{xy}u_{z,x}n_y\big)\delta u_z \\
& - (M_{xx}n_x + M_{xy}n_y)\delta u_{z,x} - (M_{yy}n_y + M_{xy}n_x)\delta u_{z,y} + (F_{xx}n_x + F_{xy}n_y)\delta\Phi_{xz} + (F_{yy}n_y + F_{xy}n_x)\delta\Phi_{yz} \Big\} \, d\Gamma,
\end{aligned}
\tag{B1a}
$$

$$
\begin{aligned}
\delta\Omega = \int_{\Gamma_u} \Big\{ & S_x(u_x - \tilde{u}_x^*)\delta u_x + S_y(u_y - \tilde{u}_x^*)\delta u_y + S_z(u_z - \tilde{u}_x^*)\delta u_z \\
& + J_{\vartheta x}\Big(u_{z,x} - \frac{6}{5h}\Phi_{xz} - \tilde{\vartheta}_x^*\Big)\Big(\delta u_{z,x} - \frac{6}{5h}\delta\Phi_{xz}\Big) + J_{\vartheta y}\Big(u_{z,y} - \frac{6}{5h}\Phi_{yz} - \tilde{\vartheta}_y^*\Big)\Big(\delta u_{z,y} - \frac{6}{5h}\delta\Phi_{yz}\Big) \Big\} \, d\Gamma \\
& + \int_{\Gamma_\Delta} \big\{ s_x(u_x - \Delta_x)\delta(u_x - \Delta_x) + s_y(u_y - \Delta_y)\delta(u_y - \Delta_y) \big\} \, d\Gamma,
\end{aligned}
\tag{B1b}
$$

and

$$
\begin{aligned}
\delta V = \int_{\Gamma_\sigma} & N_x^*\delta u_x + N_y^*\delta u_y + N_z^*\delta u_z - M_x^*\delta u_{z,x} - M_y^*\delta u_{z,y} + \frac{5}{6h}M_x^*\delta\Phi_{xz} + \frac{5}{6h}M_y^*\delta\Phi_{yz} \, d\Gamma \\
& + \int_A p^*\delta u_z \, dA + P_x^*\Delta_x + P_y^*\Delta_y.
\end{aligned}
\tag{B1c}
$$

Substituting these expressions for δU, $\delta \Omega$, and δV into (23) and enforcing the fundamental theorem of the calculus of variations leads to the equilibrium equations

$$\left\{ \begin{array}{c} N_{xx,x} + N_{xy,y} \\ N_{xy,x} + N_{yy,y} \\ M_{xx,xx} + 2M_{xy,xy} + M_{yy,yy} + N_{xx}u_{z,xx} + 2N_{xy}u_{z,xy} + N_{yy}u_{z,yy} - p^* \\ F_{xx,x} + F_{xy,y} - f_{xz} \\ F_{xy,x} + F_{yy,y} - f_{yz} \end{array} \right\} = \mathbf{0}. \tag{B2}$$

For external forces and moments applied along the boundary Γ_σ, the boundary conditions are obtained as

$$(\mathbf{b}_x + \mathbf{b}_{1x})n_x + (\mathbf{b}_y + \mathbf{b}_{1y})n_y = \mathbf{f}^*, \tag{B3}$$

where

$$\begin{aligned} \mathbf{b}_x^T &= \{N_{xx}, N_{xy}, (M_{xx,x}+M_{xy,y}), M_{xx}, M_{xy}, F_{xx}, F_{xy}\}, \\ \mathbf{b}_{1x}^T &= \{0, 0, (N_{xx}u_{z,x}+N_{xy}u_{z,y}), 0, 0, 0, 0\}, \\ \mathbf{b}_y^T &= \{N_{xy}, N_{yy}, (M_{xy,x}+M_{yy,y}), M_{xy}, M_{yy}, F_{xy}, F_{yy}\}, \\ \mathbf{b}_{1y}^T &= \{0, 0, 0, (N_{xy}u_{z,x}+N_{yy}u_{z,y}), 0, 0, 0\}, \\ \mathbf{f}^{*T} &= \left\{N_x^*, N_y^*, N_z^*, M_x^*, M_y^*, \frac{6}{5h}M_x^*, \frac{6}{5h}M_y^*\right\}. \end{aligned} \tag{B4}$$

For prescribed displacements and rotations applied through the elastic springs along the boundary Γ_u, with unit normal $\mathbf{n}$, the boundary conditions are obtained as

$$(\mathbf{c}_x + \mathbf{c}_{1x})n_x + (\mathbf{c}_y + \mathbf{c}_{1y})n_y + \mathbf{c}_u + \mathbf{c}_\Delta = \mathbf{g}_u^* + \mathbf{g}_\Delta^*, \tag{B5}$$

where

$$\begin{aligned} \mathbf{c}_x^T &= \{N_{xx}, N_{xy}, (M_{xx,x} + M_{xy,y}), -M_{xx}, -M_{xy}, F_{xx}, F_{xy}, 0, 0\}, \\ \mathbf{c}_{1x}^T &= \{0, 0, (N_{xx}u_{z,x} + N_{xy}u_{z,y}), 0, 0, 0, 0, 0, 0\}, \\ \mathbf{c}_y^T &= \{N_{xy}, N_{yy}, (M_{xy,x} + M_{yy,y}), -M_{xy}, -M_{yy}, F_{xy}, F_{yy}, 0, 0\}, \\ \mathbf{c}_{1y}^T &= \{0, 0, 0, (N_{xy}u_{z,x} + N_{yy}u_{z,y}), 0, 0, 0, 0, 0\}, \\ \mathbf{c}_u^T &= \left\{ S_x u_x, S_y u_y, S_z u_z, J_{\vartheta x}\left(u_{z,x} - \frac{6}{5h}\Phi_{xz}\right), J_{\vartheta y}\left(u_{z,y} - \frac{6}{5h}\Phi_{yz}\right), \right. \\ &\qquad \left. -\frac{6}{5h}J_{\vartheta x}\left(u_{z,x} - \frac{6}{5h}\Phi_{xz}\right), -\frac{6}{5h}J_{\vartheta y}\left(u_{z,y} - \frac{6}{5h}\Phi_{yz}\right), 0, 0\right\}, \\ \mathbf{c}_\Delta^T &= \{s_x(u_x - \Delta_x), s_y(u_y - \Delta_y), 0, 0, 0, 0, 0, s_x(\Delta_x - u_x), s_y(\Delta_y - u_y)\}, \\ \mathbf{g}_u^{*T} &= \left\{S_x \tilde{u}_x^*, S_y \tilde{u}_y^*, S_x \tilde{u}_z^*, J_{\vartheta x}\vartheta_x^*, J_{\vartheta y}\vartheta_y^*, -\frac{6}{5h}J_{\vartheta x}\vartheta_x^*, -\frac{6}{5h}J_{\vartheta y}\vartheta_y^*, 0, 0\right\}, \\ \mathbf{g}_\Delta^{*T} &= \left\{0, 0, 0, 0, 0, 0, 0, \frac{P_x^*}{L}, \frac{P_y^*}{L}\right\}. \end{aligned} \tag{B6}$$

Equations for stress analysis. The equations needed to perform a linear stress analysis are obtained by direct linearization of the nonlinear plate equations. Under the presumption of infinitesimal displacement gradients, the product terms appearing in the in-plane strains given by (7d) and the equilibrium equations given by (B2) are neglected. The resulting equilibrium equations are

$$
\left\{
\begin{array}{c}
N_{xx,x} + N_{xy,y} \\
N_{xy,x} + N_{yy,y} \\
M_{xx,xx} + 2M_{xy,xy} + M_{yy,yy} - p^* \\
F_{xx,x} + F_{xy,y} - f_{xz} \\
F_{xy,x} + F_{yy,y} - f_{yz}
\end{array}
\right\} = \mathbf{0}.
\tag{B7}
$$

Similarly, the boundary conditions on Γ_σ that are given by (B3) reduce to

$$
\boldsymbol{b}_x n_x + \boldsymbol{b}_y n_y = \boldsymbol{f}^*,
\tag{B8}
$$

where the vectors are defined as

$$
\begin{aligned}
\boldsymbol{b}_x^T &= \{N_{xx}, N_{xy}, (M_{xx,x} + M_{xy,y}), M_{xx}, M_{xy}, F_{xx}, F_{xy}\}, \\
\boldsymbol{b}_y^T &= \{N_{xy}, N_{yy}, (M_{xy,x} + M_{yy,y}), M_{xy}, M_{yy}, F_{xy}, F_{yy}\}, \\
\boldsymbol{f}^{*T} &= \left\{N_x^*, N_y^*, N_z^*, M_x^*, M_y^*, \frac{6}{5h} M_x^*, \frac{6}{5h} M_y^*\right\}.
\end{aligned}
\tag{B9}
$$

For the boundary Γ_u, the boundary conditions given by (B5) reduce to

$$
\boldsymbol{c}_x n_x + \boldsymbol{c}_y n_y + \boldsymbol{c}_u + \boldsymbol{c}_\Delta = \boldsymbol{g}_u^* + \boldsymbol{g}_\Delta^*,
\tag{B10}
$$

where the vectors are defined as

$$
\begin{aligned}
\boldsymbol{c}_x^T &= \{N_{xx}, N_{xy}, (M_{xx,x} + M_{xy,y}), -M_{xx}, -M_{xy}, F_{xx}, F_{xy}, 0, 0\}, \\
\boldsymbol{c}_y^T &= \{N_{xy}, N_{yy}, (M_{xy,x} + M_{yy,y}), -M_{xy}, -M_{yy}, F_{xy}, F_{yy}, 0, 0\}, \\
\boldsymbol{c}_u^T &= \left\{S_x u_x, S_y u_y, S_z u_z, J_{\vartheta x}\left(u_{z,x} - \frac{6}{5h}\Phi_{xz}\right), J_{\vartheta y}\left(u_{z,y} - \frac{6}{5h}\Phi_{yz}\right),\right. \\
&\qquad \left. -\frac{6}{5h} J_{\vartheta x}\left(u_{z,x} - \frac{6}{5h}\Phi_{xz}\right), -\frac{6}{5h} J_{\vartheta y}\left(u_{z,y} - \frac{6}{5h}\Phi_{yz}\right), 0, 0\right\}, \\
\boldsymbol{c}_\Delta^T &= \{s_x(u_x - \Delta_x), s_y(u_y - \Delta_y), 0, 0, 0, 0, 0, s_x(\Delta_x - u_x), s_y(\Delta_y - u_y)\}, \\
\boldsymbol{g}_u^{*T} &= \left\{S_x \tilde{u}_x^*, S_y \tilde{u}_y^*, S_x \tilde{u}_z^*, J_{\vartheta x}\vartheta_x^*, J_{\vartheta y}\vartheta_y^*, -\frac{6}{5h} J_{\vartheta x}\vartheta_x^*, -\frac{6}{5h} J_{\vartheta y}\vartheta_y^*, 0, 0\right\}, \\
\boldsymbol{g}_\Delta^{*T} &= \left\{0, 0, 0, 0, 0, 0, 0, \frac{P_x^*}{L}, \frac{P_y^*}{L}\right\}.
\end{aligned}
\tag{B11}
$$

These equations constitute a linear boundary-value problem that defines the stresses and displacements associated with stable deformations. Typically, this boundary-value problem has nonhomogeneous partial differential equations and nonhomogeneous boundary conditions.

Equations for buckling analysis. In a classical linear bifurcation analysis, the displacement field is linearized about a stable, initially flat prebuckling state. In particular, each dependent kinematic variable is partitioned into a linear prebuckling part plus an infinitesimal increment. The displacement expansions

are then substituted into the nonlinear strain-displacement relations, the linear constitutive equations, the nonlinear equilibrium equations, the boundary conditions, and the potential energy. By collecting like terms and retaining only terms that are linear in the infinitesimal increments of the dependent kinematic variables, the field equations are separated into two groups. The first group is a set of linear equations that are a subset of the equations used for the linear stress analysis in which only in-plane loads are considered and out-of-plane displacements are negligible. This linear boundary-value problem defines the in-plane stresses and displacements associated with the initial, stable prebuckling state and is referred to as the prebuckling problem.

The second group of equations, associated with infinitesimal increments in the kinematic variables, consists of homogeneous linear differential equations and homogeneous boundary conditions. Thus, these equations constitute a linear boundary-eigenvalue problem, which is referred to as the buckling problem. This type of analysis presumes that the initial prebuckling configuration of the laminate is flat, which places requirements on the nature of the applied loads. For a general in-plane loading state and multiply connected domain, the prebuckling stress state is nonuniform, with respect to the in-plane coordinates. This nonuniformity manifests itself as variable coefficients in the differential equations that define the buckling kinematic variables (incremental kinematic variables). Moreover, it is these variable coefficients that relate the buckling displacement to the magnitude of the in-plane loads.

The stable prebuckling equilibrium state of the plate is denoted by the superscript (0) while the incremental state, just after buckling occurs, is denoted by the superscript (1). It is assumed that the plate is symmetrically laminated ($\boldsymbol{B} = \boldsymbol{0}$) and remains flat prior to buckling. During the linearization procedure, no out-of-plane displacement and transverse shear deformations occur during the prebuckling state; thus, $u_z^{(0)} = 0$ and $\Phi_{xz}^{(0)} = \Phi_{yz}^{(0)} = 0$. Also, the out-of-plane displacement component in the incremental state is moderately large as compared to the incremental in-plane displacements (von Kármán assumptions are applied), that is, $u_z^{(1)} \gg u_x^{(1)}, u_y^{(1)}, \Phi_x z^{(1)}, \Phi_y z^{(1)}$. During transition to an adjacent equilibrium state, the external loads do not change and the prebuckling in-plane stresses are much higher than those in the incremental state, that is, $N_{\alpha\beta}^{(0)} \gg N_{\alpha\beta}^{(1)}$.

Prebuckling equations. In the linearization process, the terms with only superscript (0) are associated with flat stable equilibrium states and are isolated to obtain the equilibrium equations

$$\left.\begin{aligned} N_{xx,x}^{(0)} + N_{xy,y}^{(0)} \\ N_{yy,y}^{(0)} + N_{xy,x}^{(0)} \end{aligned}\right\} = 0, \tag{B12}$$

and the boundary conditions

$$\boldsymbol{b}_{0x} n_x + \boldsymbol{b}_{0y} n_y = \boldsymbol{f}_0^*, \tag{B13}$$

on the boundary, Γ_σ, in which

$$\boldsymbol{b}_{0x}^T = \left\{ N_{xx}^{(0)}, N_{xy}^{(0)} \right\}, \qquad \boldsymbol{b}_{0y}^T = \left\{ N_{xy}^{(0)}, N_{yy}^{(0)} \right\}, \qquad \boldsymbol{f}_0^{*^T} = \{ N_x^*, N_y^* \}. \tag{B14}$$

Likewise, linearization gives the boundary conditions

$$\boldsymbol{c}_{0x} n_x + \boldsymbol{c}_{0y} n_y + \boldsymbol{c}_{0u} + \boldsymbol{c}_{0\Delta} = \boldsymbol{g}_{0u}^* + \boldsymbol{g}_{0\Delta}^* \tag{B15}$$

on the boundary, Γ_u, in which

$$\boldsymbol{c}_{0x}^T = \{N_{xx}^{(0)}, N_{xy}^{(0)}, 0, 0\}, \qquad \boldsymbol{c}_{0y}^T = \{N_{xy}^{(0)}, N_{yy}^{(0)}, 0, 0\}, \qquad \boldsymbol{c}_{0s}^T = \{S_x u_x^{(0)}, S_y u_y^{(0)}, 0, 0\}, \qquad \text{(B16a)}$$

$$\boldsymbol{c}_{0\Delta}^T = \{s_x(u_x^{(0)} - \Delta_x^{(0)}), s_y(u_y^{(0)} - \Delta_y^{(0)}), s_x(\Delta_x^{(0)} - u_x^{(0)}), s_y(\Delta_y^{(0)} - u_y^{(0)})\}, \qquad \text{(B16b)}$$

$$\boldsymbol{g}_{0u}^{* \ T} = \{S_x \tilde{u}_x^{*(0)}, S_y \tilde{u}_y^{*(0)}, 0, 0\}, \qquad \boldsymbol{g}_{0\Delta}^{* \ T} = \left\{0, 0, \frac{P_x^*}{L}, \frac{P_y^*}{L}\right\}, \qquad \text{(B16c)}$$

where L represents the length of the edge mounted to the rigid bar.

Buckling equations. In the linearization process, the terms involving only superscript (1) correspond to the adjacent equilibrium state, and products of these small terms are neglected. The equilibrium equations obtained are

$$\begin{Bmatrix} N_{xx,x}^{(1)} + N_{xy,y}^{(1)} \\ N_{yy,y}^{(1)} + N_{xy,x}^{(1)} \\ M_{xx,xx}^{(1)} + 2M_{xy,xy}^{(1)} + M_{yy,yy}^{(1)} + N_{xx}^{(0)} u_{z,xx}^{(1)} + 2N_{xy}^{(0)} u_{z,xy}^{(1)} + N_{yy}^{(0)} u_{z,yy}^{(1)} \\ F_{xx,x}^{(1)} + F_{xy,y}^{(1)} - f_{xz}^{(1)} \\ F_{yy,y}^{(1)} + F_{xy,x}^{(1)} - f_{yz}^{(1)} \end{Bmatrix} = \boldsymbol{0}, \qquad \text{(B17)}$$

and the boundary conditions on the edge Γ_σ are

$$(\boldsymbol{b}_x + \boldsymbol{b}_{1x})n_x + (\boldsymbol{b}_y + \boldsymbol{b}_{1y})n_y = \boldsymbol{0}, \qquad \text{(B18)}$$

where

$$\begin{aligned} \boldsymbol{b}_x^T &= \{N_{xx}^{(1)}, N_{xy}^{(1)}, (M_{xx,x}^{(1)} + M_{xy,y}^{(1)}), M_{xx}^{(1)}, M_{xy}^{(1)}, F_{xx}^{(1)}, F_{xy}^{(1)}\}, \\ \boldsymbol{b}_y^T &= \{N_{xy}^{(1)}, N_{yy}^{(1)}, (M_{xy,x}^{(1)} + M_{yy,y}^{(1)}), M_{xy}^{(1)}, M_{yy}^{(1)}, F_{xy}^{(1)}, F_{yy}^{(1)}\}, \\ \boldsymbol{b}_{1x}^T &= \{0, 0, (N_{xx}^{(0)} u_{z,x}^{(1)} + N_{xy}^{(0)} u_{z,y}^{(1)}), 0, 0, 0, 0\}, \\ \boldsymbol{b}_{1y}^T &= \{0, 0, 0, (N_{xy}^{(1)} u_{z,x}^{(1)} + N_{yy}^{(1)} u_{z,y}^{(1)}), 0, 0, 0\}. \end{aligned} \qquad \text{(B19)}$$

Similarly, the boundary conditions on the edges Γ_u and Γ_Δ obtained from linearization are

$$(\boldsymbol{c}_x + \boldsymbol{c}_{1x})n_x + (\boldsymbol{c}_y + \boldsymbol{c}_{1y})n_y + \boldsymbol{c}_u + \boldsymbol{c}_\Delta = \boldsymbol{0}, \qquad \text{(B20)}$$

where

$$\begin{aligned} \boldsymbol{c}_x^T &= \{N_{xx}^{(1)}, N_{xy}^{(1)}, (M_{xx,x}^{(1)} + M_{xy,y}^{(1)}), -M_{xx}^{(1)}, -M_{xy}^{(1)}, F_{xx}^{(1)}, F_{xy}^{(1)}, 0, 0\}, \\ \boldsymbol{c}_{1x}^T &= \{0, 0, (N_{xx}^{(0)} u_{z,x}^{(1)} + N_{xy}^{(0)} u_{z,y}^{(1)}), 0, 0, 0, 0, 0, 0\}, \\ \boldsymbol{c}_y^T &= \{N_{xy}^{(1)}, N_{yy}^{(1)}, (M_{xy,x}^{(1)} + M_{yy,y}^{(1)}), -M_{xy}^{(1)}, -M_{yy}^{(1)}, F_{xy}^{(1)}, F_{yy}^{(1)}, 0, 0\}, \\ \boldsymbol{c}_{1y}^T &= \{0, 0, 0, (N_{xy}^{(0)} u_{z,x}^{(1)} + N_{yy}^{(0)} u_{z,y}^{(1)}), 0, 0, 0, 0, 0\}, \\ \boldsymbol{c}_u^T &= \left\{S_x u_x^{(1)}, S_y u_y^{(1)}, S_z u_z^{(1)}, J_{\vartheta x}\left(u_{z,x}^{(1)} - \frac{6}{5h}\Phi_{xz}^{(1)}\right), J_{\vartheta y}\left(u_{z,y}^{(1)} - \frac{6}{5h}\Phi_{yz}^{(1)}\right), \right. \\ &\qquad \left. -\frac{6}{5h}J_{\vartheta x}\left(u_{z,x}^{(1)} - \frac{6}{5h}\Phi_{xz}^{(1)}\right), -\frac{6}{5h}J_{\vartheta y}\left(u_{z,y}^{(1)} - \frac{6}{5h}\Phi_{yz}^{(1)}\right), 0, 0\right\}, \\ \boldsymbol{c}_\Delta^T &= \{S_x(u_x^{(1)} - \Delta_x^{(1)}), S_y(u_y^{(1)} - \Delta_y^{(1)}), 0, 0, 0, 0, 0, S_x(\Delta_x^{(1)} - u_x^{(1)}), S_y(\Delta_y^{(1)} - u_y^{(1)})\}. \end{aligned} \qquad \text{(B21)}$$

Appendix C: Representation of the displacement quantities

The local displacement quantities $\bar{u}_i$ and $\bar{\Phi}_{iz}$ that appear in (24) are specified in the form of Laurent series

$$\bar{u}_\alpha = 2h(\rho) \operatorname{Re} \sum_{\substack{n=-N \\ n \neq 0}}^{N} a_n^{(\alpha)} \xi^n, \quad \bar{u}_z = 2h(\rho) \operatorname{Re} \sum_{\substack{n=-N \\ n \neq 0}}^{N} a_n^{(z)} \int \xi^n \, d\bar{z}, \quad \bar{\Phi}_{\alpha z} = 2h(\rho) \operatorname{Re} \sum_{\substack{n=-N \\ n \neq 0}}^{N} a_n^{(\alpha z)} \xi^n$$

$$(\alpha = x, y), \quad \text{(C1)}$$

where $\bar{a}_n^{(\alpha)}$ and $\bar{a}_n^{(\alpha z)}$ are complex-valued unknown coefficients and the complex variable $\bar{z}$ is defined as $\bar{z} = x' + i y'$ with respect to the local x'-y' coordinate system shown in Figure 1. In (C1), all the series expansions are defined in terms of a complex variable ξ that is analytic outside of a unit circle and related to the complex variable $\bar{z}$ through a mapping function $\omega(\bar{z})$ as

$$\bar{z} = \omega^{-1}(\bar{z}) = r\xi - \frac{s}{\xi}. \quad \text{(C2)}$$

In this mapping, r and s are real-valued constants defined in terms of the cutout geometry as

$$r = \tfrac{1}{2}(a+b), \quad \text{(C3a)}$$

and

$$s = \tfrac{1}{2}(a-b). \quad \text{(C3b)}$$

The mapping function, $\omega(\bar{z})$, transforms the complex plane, $\bar{z}$, with an elliptic cutout to another complex plane, ξ, with an internal boundary as a unit-radius circle while the external boundaries preserve their 90 degree angles [Bowie 1956], thus enabling use of Laurent series. Furthermore, a domain-of-influence function $h(\rho)$ is defined as the fifth-order polynomial

$$h(\rho) = \begin{cases} 1 - 10\left(\dfrac{\rho}{\rho_0}\right)^3 + 15\left(\dfrac{\rho}{\rho_0}\right)^4 - 6\left(\dfrac{\rho}{\rho_0}\right)^5 & \text{if } 0 \leq \rho \leq \rho_0, \\ 0 & \text{if } \rho \geq \rho_0, \end{cases} \quad \text{(C4)}$$

in which $\rho = \sqrt{x'^2 + y'^2}$ and ρ_0 is the radius of influence of $h(\rho)$ outside the cutout (that is, $\rho_0 > \max[a, b]$). Note that the function $h(\rho)$ and its derivatives vanish for $\rho \geq \rho_0$.

The global displacement quantities $\bar{\bar{u}}_i$ and $\bar{\bar{\Phi}}_{\alpha z}$ are specified as Chebyshev series in the form

$$\bar{\bar{u}}_\alpha = \sum_{m=0}^{M} \sum_{n=0}^{m} c_{mn}^{(\alpha)} T_m(s_1) T_n(s_2), \qquad \bar{\bar{\Phi}}_{\alpha z} = \sum_{m=0}^{M} \sum_{n=0}^{m} c_{mn}^{(\alpha z)} T_m(s_1) T_n(s_2) \qquad (\alpha = x, y), \quad \text{(C5)}$$

where T_k is the kth term of the Chebyshev series with $T_{k+1}(x) = 2x T_k(x) - T_{k-1}(x)$ while $T_0(x) = 1$ and $T_1(x) = x$. The nondimensional coordinates s_1 and s_2 are defined as $s_1 = 2x/W$ and $s_2 = 2y/L$, where W and L are the characteristic width and length of the plate, respectively.

The vector of unknown generalized coordinates q that appears in (25) contains all the unknown real and complex-valued constants that appear in (C1) and (C5). Specifically,

$$q^T = \{\bar{q}_x^T, \bar{q}_y^T, \bar{q}_z^T, \bar{q}_{xz}^T, \bar{q}_{yz}^T, \bar{\bar{q}}_x^T, \bar{\bar{q}}_y^T, \bar{\bar{q}}_z^T, \bar{\bar{q}}_{xz}^T, \bar{\bar{q}}_{yz}^T\}, \quad \text{(C6)}$$

where

$$\bar{q}_\alpha^T = \{ a_{-N}^{(\alpha)\,T}, a_{-N+1}^{(\alpha)\,T}, \ldots, a_{-1}^{(\alpha)\,T}, a_1^{(\alpha)\,T}, \ldots, a_{N-1}^{(\alpha)\,T}, a_N^{(\alpha)\,T} \},$$

$$\bar{q}_{\alpha z}^T = \{ a_{-N}^{(\alpha z)\,T}, a_{-N+1}^{(\alpha z)\,T}, \ldots, a_{-1}^{(\alpha z)\,T}, a_1^{(\alpha z)\,T}, \ldots, a_{N-1}^{(\alpha z)\,T}, a_N^{(\alpha z)\,T} \},$$

$$\bar{\bar{q}}_\alpha^T = \{ c_{00}^{(\alpha)\,T}, c_{10}^{(\alpha)\,T}, c_{01}^{(\alpha)\,T}, \ldots, c_{M0}^{(\alpha)\,T}, c_{(M-1)1}^{(\alpha)\,T}, c_{(M-2)2}^{(\alpha)\,T}, \ldots, c_{1(M-1)}^{(\alpha)\,T}, c_{0M}^{(\alpha)\,T} \}, \qquad (\alpha = x, y, z).$$

$$\bar{\bar{q}}_{\alpha z}^T = \{ c_{00}^{(\alpha z)\,T}, c_{10}^{(\alpha z)\,T}, c_{01}^{(\alpha z)\,T}, \ldots, c_{M0}^{(\alpha z)\,T}, c_{(M-1)1}^{(\alpha z)\,T}, c_{(M-2)2}^{(\alpha z)\,T}, \ldots, c_{1(M-1)}^{(\alpha z)\,T}, c_{0M}^{(\alpha z)\,T} \},$$

(C7)

The corresponding vectors of known functions, V_i and $V_{\alpha z}$ ($i = x, y, z; \alpha = x, y$) in (25) for all displacement quantities are defined as

$$V_x^T = \{ \bar{V}_0^T, 0^T, 0^T, 0^T, 0^T, \bar{\bar{V}}_0^T, 0^T, 0^T, 0^T, 0^T \},$$

$$V_y^T = \{ 0^T, \bar{V}_0^T, 0^T, 0^T, 0^T, 0^T, \bar{\bar{V}}_0^T, 0^T, 0^T, 0^T \},$$

$$V_y^T = \{ 0^T, 0^T, \bar{V}_z^T, 0^T, 0^T, 0^T, 0^T, \bar{\bar{V}}_0^T, 0^T, 0^T \},$$

$$V_{xz}^T = \{ 0^T, 0^T, 0^T, \bar{V}_0^T, 0^T, 0^T, 0^T, 0^T, \bar{\bar{V}}_0^T, 0^T \},$$

$$V_{yz}^T = \{ 0^T, 0^T, 0^T, 0^T, \bar{V}_0^T, 0^T, 0^T, 0^T, 0^T, \bar{\bar{V}}_0^T \},$$

(C8)

where the vectors $\bar{V}_0$, $\bar{V}_z$, and $\bar{\bar{V}}_0$ are defined in the form

$$\bar{V}_\beta^T = \{ \bar{V}_{\beta(-N)}^T, \bar{V}_{\beta(-N+1)}^T, \ldots, \bar{V}_{\beta(-1)}^T, \bar{V}_{\beta(1)}^T, \ldots, \bar{V}_{\beta(N-1)}^T, \bar{V}_{\beta(N)}^T \} \quad (\beta = 0, z), \qquad (C9)$$

with

$$\bar{V}_{0(n)}^T = \{ 2\,\mathrm{Re}[\xi^n h(\rho)], -2\,\mathrm{Im}[\xi^n h(\rho)] \}, \tag{C10a}$$

$$\bar{V}_{z(n)}^T = \left\{ 2\,\mathrm{Re}\left[\left(\int \xi^n\, d\bar{z} \right) h(\rho) \right], -2\,\mathrm{Im}\left[\left(\int \xi^n\, d\bar{z} \right) h(\rho) \right] \right\}, \tag{C10b}$$

and

$$\bar{\bar{V}}_0^T = \{ T_0(s_1) T_0(s_2), T_1(s_1) T_0(s_2), T_0(s_1) T_1(s_2), \ldots, T_M(s_1) T_0(s_2),$$

$$T_{M-1}(s_1) T_1(s_2), \ldots, T_1(s_1) T_{M-1}(s_2), T_0(s_1) T_M(s_2) \}. \quad (C11)$$

The integral term, $\int \xi^n\, d\bar{z}$, in (C10b) is expressed as

$$\int \xi^n\, d\bar{z} = \begin{cases} r\dfrac{\xi^{n+1}}{n+1} - s\dfrac{\xi^{n-1}}{n-1} & \text{if } |n| > 1, \\[2mm] r\ln\xi + s\dfrac{\xi^{-2}}{2} & \text{if } n = -1, \\[2mm] r\dfrac{\xi^2}{2} - s\ln\xi & \text{if } n = 1. \end{cases} \tag{C12}$$

The functions chosen for representing the local displacement quantities produce multivalued modes, because of the presence of the logarithmic terms in (C12), and must be made single-valued to obtain

unique representations. In matrix form, the single-valuedness conditions are expressed as

$$G_c q = 0, \tag{C13}$$

in which G_c is the coefficient matrix of the constraint equations and is defined as

$$G_c = \begin{bmatrix} G_r \\ G_s \end{bmatrix}, \tag{C14}$$

where

$$G_r^T = \left\{ 0^T, 0^T, \ldots, 0^T, g_{(-1)}, 0^T, 0^T, \ldots, 0^T, 0^T \right\}, \tag{C15a}$$

$$G_s^T = \left\{ 0^T, 0^T, \ldots, 0^T, 0^T, g_{(1)}, 0^T, \ldots, 0^T, 0^T \right\}, \tag{C15b}$$

with

$$g_{(-1)}^T = \{0, r\}, \tag{C16a}$$

and

$$g_{(1)}^T = \{0, s\}. \tag{C16b}$$

Note that the subscripts (-1) and (1) denote the locations of the terms in the local series. Finally, the matrix constraint equations in (C13) are integrated into the total potential energy formulation via Lagrange multipliers, producing zero potential energy, in the form

$$W = \lambda^T G_c q \equiv 0, \tag{C17}$$

where W is the potential energy of constraint forces, and λ denotes the vector of unknown Lagrange multipliers given by

$$\lambda^T = \{\lambda_r, \lambda_s\}, \tag{C18}$$

where λ_r and λ_s denote the unknown constraint forces (Lagrange multipliers) that enforce the conditions in (C13).

Appendix D: Details of the solution method

Using the representations of the displacement fields in (25), the linearized form of the vector of strain quantities, e, given by (14b), is expressed in terms of the unknown generalized coordinates as

$$e = Bq, \tag{D1}$$

where the matrix B is defined as

$$B = \begin{bmatrix} B^\epsilon \\ B^\kappa \\ B^\Gamma \\ B^\Phi \end{bmatrix}, \tag{D2}$$

and the coefficient matrices $\boldsymbol{B}^\epsilon$, $\boldsymbol{B}^\kappa$, $\boldsymbol{B}^\Gamma$, and $\boldsymbol{B}^\Phi$ are defined as

$$\boldsymbol{B}^\epsilon = \begin{bmatrix} \boldsymbol{V}_{x,x}^T \\ \boldsymbol{V}_{y,y}^T \\ \boldsymbol{V}_{x,y}^T + \boldsymbol{V}_{y,x}^T \end{bmatrix}, \quad \boldsymbol{B}^\kappa = \begin{bmatrix} -\boldsymbol{V}_{z,xx}^T \\ -\boldsymbol{V}_{z,yy}^T \\ -2\boldsymbol{V}_{z,xy}^T \end{bmatrix}, \quad \boldsymbol{B}^\Gamma = \begin{bmatrix} \boldsymbol{V}_{xz,x}^T \\ \boldsymbol{V}_{yz,y}^T \\ \boldsymbol{V}_{xz,y}^T + \boldsymbol{V}_{yz,x}^T \end{bmatrix}, \quad \boldsymbol{B}^\Phi = \begin{bmatrix} \boldsymbol{V}_{xz}^T \\ \boldsymbol{V}_{yz}^T \end{bmatrix}. \tag{D3}$$

The weighted-average boundary displacement vector (19a) is also expressed in terms of the unknown generalized coordinates as

$$\tilde{\boldsymbol{u}} = \tilde{\boldsymbol{V}}_B \boldsymbol{q}, \tag{D4}$$

where the matrix $\tilde{\boldsymbol{V}}_B$ is defined as

$$\tilde{\boldsymbol{V}}_B = \begin{bmatrix} \boldsymbol{V}_x^T \\ \boldsymbol{V}_y^T \\ \boldsymbol{V}_z^T \\ \boldsymbol{V}_{z,x}^T - \frac{6}{5}\boldsymbol{V}_{xz}^T \\ \boldsymbol{V}_{z,y}^T - \frac{6}{5}\boldsymbol{V}_{yz}^T \end{bmatrix}. \tag{D5}$$

Substituting the matrix representation of $\boldsymbol{e}$ given by (D1) into the strain energy expression for the laminate defined by (17) and rearranging the terms, the linearized form of the strain energy is expressed in terms of the unknown generalized coordinates as

$$U = \frac{1}{2}\boldsymbol{q}^T \boldsymbol{K}_C \boldsymbol{q}, \tag{D6}$$

where the matrix $\boldsymbol{K}_C$ is defined as

$$\boldsymbol{K}_C = \int_A \boldsymbol{B}^T \boldsymbol{C} \boldsymbol{B} \, dA. \tag{D7}$$

Substituting (D4) for the boundary displacement vector $\tilde{\boldsymbol{u}}$ into the strain energy of the elastic spring supports, given by (18) and rearranging the terms, the linearized form of the strain energy Ω is expressed in terms of the unknown generalized coordinates as

$$\Omega = \frac{1}{2}\boldsymbol{q}^T \boldsymbol{S}_{qq} \boldsymbol{q} - \boldsymbol{q}^T \boldsymbol{S}_q^* + \Omega^*, \tag{D8}$$

where the matrix $\boldsymbol{S}_{qq}$ and the vector $\boldsymbol{S}_q^*$ are defined as

$$\boldsymbol{S}_{qq} = \int_{\Gamma_u} \tilde{\boldsymbol{V}}_B^T \boldsymbol{k}_u \tilde{\boldsymbol{V}}_B \, d\Gamma \tag{D9a}$$

and

$$\boldsymbol{S}_q^* = \int_{\Gamma_u} \tilde{\boldsymbol{V}}_B^T \boldsymbol{k}_u \tilde{\boldsymbol{u}}^* \, d\Gamma. \tag{D9b}$$

The strain energy of the elastic spring arising from the applied displacement constraints Ω^* is written as

$$\Omega^* = \frac{1}{2} \int_{\Gamma_u} \tilde{\boldsymbol{u}}^{*T} \boldsymbol{k}_u \tilde{\boldsymbol{u}}^* \, d\Gamma. \tag{D10}$$

Substituting (D4) and the transverse displacement u_z given by (25a) into the potential energy of external loads given by (21) and rearranging the terms, the linearized form of the potential energy V is expressed

in terms of the unknown generalized coordinates as

$$V = -\boldsymbol{q}^T \boldsymbol{N}^* - \boldsymbol{q}^T \boldsymbol{p}_z^*, \tag{D11}$$

where the vectors $\boldsymbol{N}^*$ and $\boldsymbol{p}_z^*$ are defined as

$$\boldsymbol{N}^* = \int_{\Gamma^{(\sigma)}} \tilde{\boldsymbol{V}}_B^T \boldsymbol{T}^* \, d\Gamma, \qquad \boldsymbol{p}_z^* = \int_A p^* \boldsymbol{V}_z \, dA. \tag{D12}$$

Appendix E: Details of the bifurcation analysis

In the bifurcation analysis, the displacement vector $\boldsymbol{u}$, weighted-average boundary displacement vector $\tilde{\boldsymbol{u}}$, vector of generalized coordinates $\boldsymbol{q}$, uniform-edge-displacement vector $\boldsymbol{\Delta}$, and constraint force vector $\boldsymbol{\lambda}$ are expressed as

$$\boldsymbol{u} = \boldsymbol{u}^{(0)} + e\boldsymbol{u}^{(1)}, \tag{E1a}$$

$$\tilde{\boldsymbol{u}} = \tilde{\boldsymbol{u}}^{(0)} + e\tilde{\boldsymbol{u}}^{(1)}, \tag{E1b}$$

$$\boldsymbol{q} = \boldsymbol{q}^{(0)} + e\boldsymbol{q}^{(1)}, \tag{E1c}$$

$$\boldsymbol{\Delta} = \boldsymbol{\Delta}^{(0)} + e\boldsymbol{\Delta}^{(1)}, \tag{E1d}$$

$$\boldsymbol{\lambda} = \boldsymbol{\lambda}^{(0)} + e\boldsymbol{\lambda}^{(1)}. \tag{E1e}$$

By using these expressions, the terms appearing in the potential energy expansion given by (31) are obtained as

$$\pi^{(0)}\big(\boldsymbol{Q}^{(0)}\big) = U^{(0)}\big(\boldsymbol{q}^{(0)}\big) + \Omega^{(0)}\big(\boldsymbol{q}^{(0)}, \boldsymbol{\Delta}^{(0)}\big) + V^{(0)}\big(\boldsymbol{q}^{(0)}, \boldsymbol{\Delta}^{(0)}\big) + W^{(0)}\big(\boldsymbol{q}^{(0)}, \boldsymbol{\lambda}^{(0)}\big), \tag{E2a}$$

$$\pi^{(1)}\big(\boldsymbol{Q}^{(0)}, \boldsymbol{Q}^{(1)}\big) = U^{(1)}\big(\boldsymbol{q}^{(0)}, \boldsymbol{q}^{(1)}\big) + \Omega^{(1)}\big(\boldsymbol{q}^{(0)}, \boldsymbol{\Delta}^{(0)}, \boldsymbol{q}^{(1)}, \boldsymbol{\Delta}^{(1)}\big)$$
$$+ V^{(1)}\big(\boldsymbol{q}^{(0)}, \boldsymbol{\Delta}^{(0)}, \boldsymbol{q}^{(1)}, \boldsymbol{\Delta}^{(1)}\big) + W^{(1)}\big(\boldsymbol{q}^{(0)}, \boldsymbol{\lambda}^{(0)}, \boldsymbol{q}^{(1)}, \boldsymbol{\lambda}^{(1)}\big), \tag{E2b}$$

$$\pi^{(2)}\big(\boldsymbol{Q}^{(0)}, \boldsymbol{Q}^{(1)}\big) = U^{(1)}\big(\boldsymbol{q}^{(0)}, \boldsymbol{q}^{(1)}\big) + \Omega^{(1)}\big(\boldsymbol{q}^{(1)}, \boldsymbol{\Delta}^{(1)}\big) + W^{(1)}\big(\boldsymbol{q}^{(1)}, \boldsymbol{\lambda}^{(1)}\big). \tag{E2c}$$

The corresponding displacement vectors for the prebuckling and adjacent equilibrium states, $\boldsymbol{u}^{(0)}$ and $\boldsymbol{u}^{(1)}$, are given by

$$\boldsymbol{u}^{(0)T} = \big\{ u_x^{(0)}, u_y^{(0)}, 0, 0, 0, 0, 0 \big\}, \tag{E3}$$

$$\boldsymbol{u}^{(1)T} = \big\{ u_x^{(1)}, u_y^{(1)}, u_z^{(1)}, \Phi_{xz}^{(1)}, \Phi_{yz}^{(1)}, u_{z,x}^{(1)}, u_{z,y}^{(1)} \big\}. \tag{E4}$$

The zero values in (E3) indicate an absence of bending deformations in the prebuckling equilibrium state. The strain vector $\boldsymbol{e}$, defined by (14b), becomes

$$\boldsymbol{e}(x, y) = \boldsymbol{e}^{(0)}(x, y) + e\boldsymbol{e}^{(1)}(x, y) + e^2\boldsymbol{e}^{(2)}(x, y) + O(e^3), \tag{E5}$$

where third-order terms in the parameter e are disregarded. The first three terms in (E5) are given by

$$e^{(0)T} = \left\{ u_{x,x}^{(0)}, u_{y,y}^{(0)}, u_{x,y}^{(0)} + u_{y,x}^{(0)}, 0, 0, 0, 0, 0, 0, 0, 0 \right\}, \tag{E6a}$$

$$e^{(1)T} = \left\{ u_{x,x}^{(1)}, u_{y,y}^{(1)}, u_{x,y}^{(1)} + u_{y,x}^{(1)}, -u_{z,xx}^{(1)}, -u_{z,yy}^{(1)}, -2u_{z,xy}^{(1)}, \Phi_{xz,x}^{(1)}, \Phi_{yz,y}^{(1)}, \Phi_{xz,y}^{(1)} + \Phi_{yz,x}^{(1)}, \Phi_{xz}^{(1)}, \Phi_{yz}^{(1)} \right\}, \tag{E6b}$$

$$e^{(2)T} = \tfrac{1}{2} \left\{ \left(u_{z,x}^{(1)} \right)^2, \left(u_{z,y}^{(1)} \right)^2, 2u_{z,x}^{(1)} u_{z,y}^{(1)}, 0, 0, 0, 0, 0, 0, 0, 0 \right\}. \tag{E6c}$$

Applying the bifurcation procedure to (25), the displacement quantities $u_i\,(i = x, y, z)$ and $\Phi_{iz}\,(i = x, y)$ for each state are found to be

$$u_i^{(k)} = \boldsymbol{V}_i^T \boldsymbol{q}^{(k)} \quad \text{with } i = x, y, z, \qquad \Phi_{iz}^{(k)} = \boldsymbol{V}_{iz}^T \boldsymbol{q}^{(k)} \quad \text{with } i = x, y, \tag{E7}$$

in which $k = 0, 1$. Using these representations, the strain vectors $e^{(0)}$, $e^{(1)}$, and $e^{(2)}$ are rewritten in matrix form in terms of the unknown generalized coordinates as

$$e^{(0)} = \boldsymbol{B}_L \boldsymbol{q}^{(0)}, \qquad e^{(1)} = \boldsymbol{B} \boldsymbol{q}^{(1)}, \qquad e_N^{(1)} = \boldsymbol{B}_N \boldsymbol{q}^{(1)}, \tag{E8}$$

where the matrices $\boldsymbol{B}_L$ and $\boldsymbol{B}_N$ are defined as

$$\boldsymbol{B}_L = \begin{bmatrix} \boldsymbol{B}^{\epsilon} \\ \boldsymbol{0} \\ \boldsymbol{0} \\ \boldsymbol{0} \end{bmatrix}, \qquad \boldsymbol{B}_N = \begin{bmatrix} \boldsymbol{B}_N^{\epsilon} \\ \boldsymbol{0} \\ \boldsymbol{0} \\ \boldsymbol{0} \end{bmatrix}, \tag{E9}$$

and the coefficient matrix $\boldsymbol{B}_N^{\epsilon}$ is defined as

$$\boldsymbol{B}_N^{\epsilon} = \begin{bmatrix} \boldsymbol{V}_{z,x}^T \\ \boldsymbol{V}_{z,y}^T \end{bmatrix}. \tag{E10}$$

Substituting (E5) into the constitutive equations given by (15) yields

$$s(x, y) = s^{(0)}(x, y) + e s^{(1)}(x, y) + e^2 s^{(2)}(x, y) + O(e^3), \tag{E11}$$

where

$$s^{(0)} = \boldsymbol{C} e^{(0)}, \qquad s^{(1)} = \boldsymbol{C} e^{(1)}, \qquad s^{(2)} = \boldsymbol{C} e^{(2)}, \tag{E12}$$

and $\boldsymbol{C}$ is for symmetrically laminated plates, that is,

$$\boldsymbol{C} = \begin{bmatrix} A & 0 & 0 & 0 \\ 0 & D & F & 0 \\ 0 & F & H & 0 \\ 0 & 0 & 0 & G \end{bmatrix}. \tag{E13}$$

Thus, the stress resultant vector for each state becomes

$$s^{(0)T} = \left\{ N_{xx}^{(0)}, N_{yy}^{(0)}, N_{xy}^{(0)}, 0, 0, 0, 0, 0, 0, 0, 0 \right\}, \tag{E14a}$$

$$s^{(1)T} = \left\{ N_{xx}^{(1)}, N_{yy}^{(1)}, N_{xy}^{(1)}, M_{xx}^{(1)}, M_{yy}^{(1)}, M_{xy}^{(1)}, F_{xx}^{(1)}, F_{yy}^{(1)}, F_{xy}^{(1)}, q_{xz}^{(1)}, q_{yz}^{(1)} \right\}, \tag{E14b}$$

and $s^{(2)}$ involves only the contribution of the matrix A and the nonlinear components of the in-plane strains appearing in (E6c).

Next, substituting (E5) and (E11) into (13) and noting that $s^{(k)T}e^{(j)} = s^{(j)T}e^{(k)}$ gives the strain energy expansion

$$U = U^{(0)} + eU^{(1)} + e^2 U^{(2)} + O(e^3),$$ (E15)

where

$$
\begin{aligned}
U^{(0)} &= \frac{1}{2} \iint_A e^{(0)T} C e^{(0)} \, dx \, dy, \\
U^{(1)} &= \iint_A s^{(1)T} e^{(0)} \, dx \, dy, \\
U^{(2)} &= \iint_A \left(\frac{1}{2} e^{(1)T} C e^{(1)} + s^{(0)T} e^{(2)} \right) dx \, dy.
\end{aligned}
$$ (E16)

The terms $U^{(1)}$ and $U^{(2)}$ represent the first and second variations of the strain energy, respectively. It is convenient to represent the second term of $U^{(2)}$ as the quadratic form

$$s^{(0)T} e^{(2)} = e_N^{(1)T} N^{(0)} e_N^{(1)},$$ (E17)

where

$$e_N^{(1)T} = \{u_{z,x}^{(1)}, u_{z,y}^{(1)}\}, \qquad N^{(0)} = \begin{bmatrix} N_{xx}^{(0)} & N_{xy}^{(0)} \\ N_{xy}^{(0)} & N_{yy}^{(0)} \end{bmatrix},$$ (E18)

leading to

$$U^{(2)} = \iint_A \left(\frac{1}{2} e^{(1)T} C e^{(1)} + e_N^{(1)T} N^{(0)} e_N^{(1)} \right) dx \, dy.$$ (E19)

Substituting for the matrix representation of the strain resultant vectors $e^{(k)}$ ($k = 0, 1, 2$) given by (E8) into the strain energy expression given by (E16) and rearranging the terms, the expressions for $U^{(k)}$ ($k = 0, 1, 2$) are expressed in terms of the unknown generalized coordinates as

$$
\begin{aligned}
U^{(0)} &= \tfrac{1}{2} q^{(0)T} K_{L0} q^{(0)}, \qquad U^{(1)} = -\tfrac{1}{2} q^{(0)T} K_{L01} q^{(1)} - \tfrac{1}{2} q^{(0)T} K_{L01}^T q^{(1)}, \\
U^{(2)} &= \tfrac{1}{2} q^{(1)T} K_{L1} q^{(1)} + \tfrac{1}{2} q^{(1)T} H q^{(1)},
\end{aligned}
$$ (E20)

where the matrices K_{L0}, K_{L1}, K_{L01}, and H are defined as

$$
\begin{aligned}
K_{L0} &= \int_A B_{L0}^T C B_{L0} \, dA, \qquad K_{L1} = \int_A B_{L1}^T C B_{L1} \, dA, \\
K_{L01} &= \int_A B_{L0}^T C B_{L1} \, dA, \qquad H = \int_A B_N^T N^{(0)} B_N \, dA.
\end{aligned}
$$ (E21)

Similarly, substituting (E1b) into the expression for the strain energy of the elastic spring supports given by (18) results in

$$\Omega = \Omega^{(0)} + e\Omega^{(1)} + e^2 \Omega^{(2)},$$ (E22)

where

$$\Omega^{(0)} = \frac{1}{2} \int_{\Gamma_u} \left(\tilde{\boldsymbol{u}}^{(0)} - \tilde{\boldsymbol{u}}^* \right)^T \boldsymbol{k}_u \left(\tilde{\boldsymbol{u}}^{(0)} - \tilde{\boldsymbol{u}}^* \right) d\Gamma + \frac{1}{2} \int_{\Gamma_\Delta} \left(\tilde{\boldsymbol{u}}^{(0)} - \boldsymbol{\Delta}^{(0)} \right)^T \boldsymbol{k}_u \left(\tilde{\boldsymbol{u}}^{(0)} - \boldsymbol{\Delta}^{(0)} \right) d\Gamma, \tag{E23a}$$

$$\Omega^{(1)} = \int_{\Gamma_u} \left(\tilde{\boldsymbol{u}}^{(0)} - \tilde{\boldsymbol{u}}^* \right)^T \boldsymbol{k}_u \tilde{\boldsymbol{u}}^{(1)} \, d\Gamma + \int_{\Gamma_\Delta} \left(\tilde{\boldsymbol{u}}^{(1)} - \boldsymbol{\Delta}^{(1)} \right)^T \boldsymbol{k}_u \left(\tilde{\boldsymbol{u}}^{(0)} - \boldsymbol{\Delta}^{(0)} \right) d\Gamma, \tag{E23b}$$

$$\Omega^{(2)} = \frac{1}{2} \int_{\Gamma_u} \tilde{\boldsymbol{u}}^{(1)T} \boldsymbol{k}_u \tilde{\boldsymbol{u}}^{(1)} \, d\Gamma + \frac{1}{2} \int_{\Gamma_\Delta} \left(\tilde{\boldsymbol{u}}^{(1)} - \boldsymbol{\Delta}^{(1)} \right)^T \boldsymbol{k}_u \left(\tilde{\boldsymbol{u}}^{(1)} - \boldsymbol{\Delta}^{(1)} \right) d\Gamma. \tag{E23c}$$

Substituting for the vector representation of the weighted-average boundary displacement field $\tilde{\boldsymbol{u}}$, given by (D4), the expressions for $\Omega^{(k)}$ are rewritten as

$$\Omega^{(0)} = \tfrac{1}{2} \boldsymbol{q}^{(0)T} \boldsymbol{S}_{qq} \boldsymbol{q}^{(0)} - \boldsymbol{q}^{(0)T} \boldsymbol{S}_q^* + \Omega^* + \tfrac{1}{2} \boldsymbol{\Delta}^{(0)T} \boldsymbol{s}_{\Delta\Delta} \boldsymbol{\Delta}^{(0)} \tag{E24a}$$

$$- \tfrac{1}{2} \boldsymbol{\Delta}^{(0)T} \boldsymbol{s}_{q\Delta}^T \boldsymbol{q}^{(0)} - \tfrac{1}{2} \boldsymbol{q}^{(0)T} \boldsymbol{s}_{q\Delta} \boldsymbol{\Delta}^{(0)} + \tfrac{1}{2} \boldsymbol{q}^{(0)T} \boldsymbol{S}_{\Delta\Delta} \boldsymbol{q}^{(0)}, \tag{E24b}$$

$$\Omega^{(1)} = \boldsymbol{q}^{(0)T} \boldsymbol{S}_{qq} \boldsymbol{q}^{(1)} - \boldsymbol{q}^{(1)T} \boldsymbol{S}_q^* + \boldsymbol{\Delta}^{(1)T} \boldsymbol{s}_{\Delta\Delta} \boldsymbol{\Delta}^{(0)} - \boldsymbol{\Delta}^{(1)T} \boldsymbol{s}_{q\Delta}^T \boldsymbol{q}^{(0)} - \boldsymbol{q}^{(1)T} \boldsymbol{s}_{q\Delta} \boldsymbol{\Delta}^{(0)} + \boldsymbol{q}^{(1)T} \boldsymbol{S}_{\Delta\Delta} \boldsymbol{q}^{(0)}, \tag{E24c}$$

$$\Omega^{(2)} = \tfrac{1}{2} \boldsymbol{q}^{(1)T} \boldsymbol{S}_{qq} \boldsymbol{q}^{(1)} + \tfrac{1}{2} \boldsymbol{\Delta}^{(1)T} \boldsymbol{s}_{\Delta\Delta} \boldsymbol{\Delta}^{(1)} - \tfrac{1}{2} \boldsymbol{\Delta}^{(1)T} \boldsymbol{s}_{q\Delta}^T \boldsymbol{q}^{(1)} - \tfrac{1}{2} \boldsymbol{q}^{(1)T} \boldsymbol{s}_{q\Delta} \boldsymbol{\Delta}^{(1)} + \tfrac{1}{2} \boldsymbol{q}^{(1)T} \boldsymbol{S}_{\Delta\Delta} \boldsymbol{q}^{(1)}, \tag{E24d}$$

where the matrices $\boldsymbol{S}_{\Delta\Delta}$, $\boldsymbol{s}_{\Delta\Delta}$, and $\boldsymbol{s}_{q\Delta}$ are defined as

$$\boldsymbol{S}_{\Delta\Delta} = \int_{\Gamma_\Delta} \tilde{\boldsymbol{V}}_B^T \boldsymbol{k}_\Delta \tilde{\boldsymbol{V}}_B \, d\Gamma, \qquad \boldsymbol{s}_{\Delta\Delta} = \int_{\Gamma_\Delta} \boldsymbol{k}_\Delta \, d\Gamma, \qquad \boldsymbol{s}_{q\Delta} = \int_{\Gamma_\Delta} \tilde{\boldsymbol{V}}_B^T \boldsymbol{k}_\Delta \, d\Gamma. \tag{E25}$$

In these integrals, Γ_Δ represents the boundary segment having extensional springs that remain between the laminate boundary and the rigid bar.

Substituting (E1a) into the potential energy given by (21) with only the in-plane external forces acting along the edges of the laminate included gives

$$V = \left(V_\sigma^{(0)} + e V_\sigma^{(1)} \right) + \left(V_\Delta^{(0)} + e V_\Delta^{(1)} \right), \tag{E26}$$

where

$$V_\sigma^{(0)} = \int_{\Gamma_\sigma} \boldsymbol{T}^{*T} \tilde{\boldsymbol{u}}^{(0)} \, d\Gamma, \qquad V_\sigma^{(1)} = \int_{\Gamma_\sigma} \boldsymbol{T}^{*T} \tilde{\boldsymbol{u}}^{(1)} \, d\Gamma, \tag{E27}$$

and

$$V_\Delta^{(k)} = \boldsymbol{P}^{*T} \boldsymbol{\Delta}^{(k)} \quad \text{on } \Gamma_\Delta \text{ with } k = 0, 1. \tag{E28}$$

In these integrals, $\boldsymbol{T}^{*T} = \{N_x^*, N_y^*, 0, 0, 0\}$. Note that only the in-plane loads, N_x^* and N_y^*, are included in vector $\boldsymbol{T}^*$ in order to avoid bending deformations in the prebuckling state. Substituting the vector representation of the weighted-average boundary displacement field $\tilde{\boldsymbol{u}}$ into (E27), the linearized forms of the potential energy of elastic restraints, $V_\sigma^{(k)}$, are rewritten as

$$V_\sigma^{(k)} = \boldsymbol{q}^{(k)T} \boldsymbol{N}^* \quad \text{with } k = 0, 1. \tag{E29}$$

The vector $\boldsymbol{N}^*$ is defined as

$$\boldsymbol{N}^{*T} = \int_{\Gamma_\sigma} \tilde{\boldsymbol{V}}_B^T \boldsymbol{T}^* \, d\Gamma. \tag{E30}$$

The zeroth, first, and second variations of the constraint forces are obtained by substituting the vector of unknown generalized coordinates given by (E1c) and (E1e) into (C17) and rearranging the terms. This process yields

$$W^{(0)} = \boldsymbol{\lambda}^{(0)T} \boldsymbol{G}_c \boldsymbol{q}^{(0)}, \qquad W^{(1)} = \boldsymbol{\lambda}^{(0)T} \boldsymbol{G}_c \boldsymbol{q}^{(1)} + \boldsymbol{\lambda}^{(1)T} \boldsymbol{G}_c \boldsymbol{q}^{(0)}, \qquad W^{(2)} = \boldsymbol{\lambda}^{(1)T} \boldsymbol{G}_c \boldsymbol{q}^{(1)}. \qquad \text{(E31)}$$

References

[Altenbach 1998] H. Altenbach, "Theories for laminated and sandwich plates: a review", *Mech. Compos. Mater.* **34**:3 (1998), 243–252.

[Barut and Madenci 2001] A. Barut and E. Madenci, "A complex potential-variational formulation for buckling analysis of flat laminates with multiple cutouts", in *42nd AIAA/ASME/ASCE/AHS/ASC Structures, Structural Dynamics, and Materials Conference* (Seattle, WA, 2001), AIAA, Reston, VA, 2001. AIAA Paper 2001-1547.

[Barut et al. 1998] A. Barut, E. Madenci, and A. Tessler, "Analysis of composite sandwich panels via a triangular shell element based on higher-order theory", pp. 263–278 in *Sandwich construction 4: proceedings of the Fourth International Conference on Sandwich Construction* (Stockholm, 1998), edited by K.-A. Olsson, Engineering Materials Advisory Services, Cradley Heath, 1998.

[Barut et al. 2002] A. Barut, E. Madenci, T. Anderson, and A. Tessler, "Equivalent single-layer theory for a complete stress field in sandwich panels under arbitrarily distributed loading", *Compos. Struct.* **58**:4 (2002), 483–495.

[Bosia et al. 2002] F. Bosia, T. Gmür, and J. Botsis, "Deformation characteristics of composite laminates, II: An experimental/numerical study on equivalent single-layer theories", *Compos. Sci. Technol.* **62**:1 (2002), 55–66.

[Bowie 1956] O. L. Bowie, "Analysis of an infinite plate containing radial cracks originating at the boundary of an internal circular hole", *J. Math. Phys.* (*MIT*) **35** (1956), 60–71.

[Brush and Almroth 1975] D. O. Brush and B. O. Almroth, *Buckling of bars, plates and shells*, McGraw-Hill, New York, 1975.

[Demasi and Yu 2009] L. Demasi and W. Yu, "Assess the accuracy of the variational asymptotic plate and shell analysis (VAPAS) using the generalized unified formulation (GUF)", in *50th AIAA/ASME/ASCE/AHS/ASC Structures, Structural Dynamics, and Materials Conference* (Palm Springs, CA, 2009), AIAA, Reston, VA, 2009. AIAA Paper 2009-2417.

[Fung and Tong 2001] F. C. Fung and P. Tong, *Classical and computational solid mechanics*, World Scientific, River Edge, NJ, 2001.

[Ghugal and Shimpi 2002] Y. M. Ghugal and R. P. Shimpi, "A review of refined shear deformation theories of isotropic and anisotropic laminated plates", *J. Reinf. Plast. Compos.* **21**:9 (2002), 775–813.

[Iyengar and Chakraborty 2004] N. G. R. Iyengar and A. Chakraborty, "Study of interaction curves for composite laminate subjected to in-plane uniaxial and shear loadings", *Compos. Struct.* **64**:3–4 (2004), 307–315.

[Jones 1975] R. M. Jones, *Mechanics of composite materials*, McGraw-Hill, Washington, DC, 1975.

[Krishna Murty 1987] A. V. Krishna Murty, "Flexure of composite plates", *Compos. Struct.* **7**:3 (1987), 161–177.

[Liu and Li 1996] D. Liu and X. Li, "An overall view of laminate theories based on displacement hypothesis", *J. Compos. Mater.* **30**:14 (1996), 1539–1561.

[Nemeth 1990] M. P. Nemeth, "Buckling and postbuckling behavior of square compression-loaded graphite-epoxy plates with circular cutouts", NASA Technical Paper 3007, Langley Research Center, Hampton, VA, 1990, Available at http://ntrs.nasa.gov/search.jsp?R=19900016761.

[Noor and Malik 2000] A. K. Noor and M. Malik, "An assessment of five modeling approaches for thermo-mechanical stress analysis of laminated composite panels", *Comput. Mech.* **25**:1 (2000), 43–58.

[Ramm 2000] E. Ramm, "From Reissner plate theory to three dimensions in large deformation shell analysis", *Z. Angew. Math. Mech.* **80**:1 (2000), 61–68.

[Ray 2003] M. C. Ray, "Zeroth-order shear deformation theory for laminated composite plates", *J. Appl. Mech.* (*ASME*) **70**:3 (2003), 374–380.

[Reddy 1984] J. N. Reddy, "A simple higher-order theory for laminated composite plates", *J. Appl. Mech.* (*ASME*) **51**:4 (1984), 745–752.

[Reddy 1987] J. N. Reddy, "A small strain and moderate rotation theory of elastic anisotropic plates", *J. Appl. Mech.* (*ASME*) **54**:3 (1987), 623–626.

[Reddy 1990] J. N. Reddy, "A general non-linear third-order theory of plates with moderate thickness", *Int. J. Non-Linear Mech.* **25**:6 (1990), 677–686.

[Reddy 1997] J. N. Reddy, *Mechanics of laminated composite plates*, CRC Press, Boca Raton, FL, 1997.

[Reissner 1944] E. Reissner, "On the theory of bending of elastic plates", *J. Math. Phys.* (*MIT*) **23** (1944), 184–191.

[Reissner 1945] E. Reissner, "The effect of transverse shear deformation on the bending of elastic plates", *J. Appl. Mech.* (*ASME*) **12** (1945), A69–A77.

[Rohwer et al. 2001] K. Rohwer, R. Rolfes, and H. Sparr, "Higher-order theories for thermal stresses in layered plates", *Int. J. Solids Struct.* **38**:21 (2001), 3673–3687.

[Senthilnathan et al. 1987] N. R. Senthilnathan, S. P. Lim, K. H. Lee, and S. T. Chow, "Buckling of shear-deformable plates", *AIAA J.* **25**:9 (1987), 1268–1271.

[Shi 2007] G. Shi, "A new simple third-order shear deformation theory of plates", *Int. J. Solids Struct.* **44**:13 (2007), 4399–4417.

[Shimpi 1999] R. C. Shimpi, "Zeroth-order shear deformation theory for plates", *AIAA J.* **37**:4 (1999), 524–526.

[Shu and Sun 1994] X. Shu and L. Sun, "Thermomechanical buckling of laminated composite plates with higher-order transverse shear deformation", *Comput. Struct.* **53**:1 (1994), 1–7.

[Singh et al. 1994] G. Singh, G. Venkateswara Rao, and N. G. R. Iyengar, "Geometrically nonlinear flexural response characteristics of shear deformable unsymmetrically laminated plates", *Comput. Struct.* **53**:1 (1994), 69–81.

[Soldatos and Timarci 1993] K. P. Soldatos and T. Timarci, "A unified formulation of laminated composite, shear deformable, five-degrees-of-freedom cylindrical shell theories", *Compos. Struct.* **25**:1–4 (1993), 165–171.

[Sun and Hsu 1990] L. X. Sun and T. R. Hsu, "Thermal buckling of laminated composite plates with transverse shear deformation", *Comput. Struct.* **36**:5 (1990), 883–889.

[Tessler 1993] A. Tessler, "An improved plate theory of {1, 2}-order for thick composite laminates", *Int. J. Solids Struct.* **30**:7 (1993), 981–1000.

[Tessler and Saether 1991] A. Tessler and E. Saether, "A computationally viable higher-order theory for laminated composit plates", *Int. J. Numer. Methods Eng.* **31**:6 (1991), 1069–1086.

[Tessler et al. 2009] A. Tessler, M. Di Sciuva, and M. Gherlone, "A refined zigzag beam theory for composite and sandwich beams", *J. Compos. Mater.* **43**:9 (2009), 1051–1081.

[Timarci and Aydogdu 2005] T. Timarci and M. Aydogdu, "Buckling of symmetric cross-ply square plates with various boundary conditions", *Compos. Struct.* **68**:4 (2005), 381–389.

[Voyiadjis and Shi 1991] G. Z. Voyiadjis and G. Shi, "A refined two-dimensional theory for thick cylindrical shells", *Int. J. Solids Struct.* **27**:3 (1991), 261–282.

[Whitney and Nuismer 1974] J. M. Whitney and R. J. Nuismer, "Stress fracture criteria for laminated composites containing stress concentrations", *J. Compos. Mater.* **8**:3 (1974), 253–265.

[Yu and Hodges 2004] W. Yu and D. H. Hodges, "Asymptotic approach for thermoelastic analysis of laminated composite plates", *J. Eng. Mech.* (*ASCE*) **130**:5 (2004), 531–540.

ATILA BARUT: atila@email.arizona.edu
Department of Aerospace and Mechanical Engineering, The University of Arizona, Tucson, AZ 85721, United States

ERDOGAN MADENCI: madenci@email.arizona.edu
Department of Aerospace and Mechanical Engineering, The University of Arizona, Tucson, AZ 85721, United States

MICHAEL P. NEMETH: michael.p.nemeth@nasa.gov
Structural Mechanics and Concepts Branch, NASA Langley Research Center, Hampton, VA 23681-2199, United States

JOURNAL OF MECHANICS OF MATERIALS AND STRUCTURES

jomms.org

Founded by Charles R. Steele and Marie-Louise Steele

Cover design: Alex Scorpan   Cover photo: Ev Shafrir